GPI-anchored FGF directs cytoneme-mediated bidirectional signaling to self-regulate tissue-specific dispersion

Lijuan Du, Alex Sohr, Yujia Li, Sougata Roy*

Department of Cell Biology and Molecular Genetics; University of Maryland, College Park, MD 20742

*Corresponding author: sougata@umd.edu

Keywords: FGF, bidirectional signaling, GPI anchor, cytonemes, synapse, self-organization, Bnl, cell-adhesion-molecule (CAM), *Drosophila*

Short Title: Bidirectional FGF-FGFR signaling at cytoneme contacts

ABSTRACT

How signaling proteins generate a multitude of information to organize tissue patterns is critical to understanding morphogenesis. In *Drosophila*, FGF produced in wing-disc cells regulates the development of the disc-associated air-sac-primordium/ASP. We discovered that FGF is GPI-anchored to the producing cell surface and that this modification both inhibits free FGF secretion and activates target-specific bidirectional FGF-FGFR signaling through cytonemes. Source and ASP cells extend cytonemes that present FGF and FGFR on their surfaces and reciprocally recognize each other over distance by contacting each other through CAM-like FGF-FGFR binding. Contact-mediated FGF-FGFR binding induces bidirectional signaling, which, in turn, promotes ASP and source cells to polarize cytonemes toward each other and reinforce signaling contacts. Subsequent un-anchoring of FGFR-bound-FGF from the source membrane dissociates cytoneme contacts and delivers FGF target-specifically to ASP cytonemes for paracrine functions. Thus, GPI-anchored FGF organizes both source and recipient cells and self-regulates its cytoneme-mediated tissue-specific dispersion and signaling.

Introduction

During development, intercellular communication of morphogens is critical for embryonic cells to determine their positional identity, directionality, and interactions in a highly organized pattern to sculpt tissues. These conserved families of secreted morphogens/signals, such as Fibroblast Growth Factor (FGF), Hedgehog (Hh), Wingless (Wg)/Wnt, Epidermal Growth Factor (EGF), and Decapentaplegic (Dpp - a BMP homolog), act away from their sources and, upon binding to receptors, activate gene regulatory pathways to induce functions in recipient cells [1,2]. Strikingly, each signal and signaling pathway can generate a wide range of cell types and organizations in diverse developmental contexts [3]. Understanding how signals might inform cells of their positional identity, directionality, and interactions and organize these functions in diverse tissue-specific patterns is critical to understanding morphogenesis.

The discrete tissue-specific organization of morphogen signaling is known to be dependent on the ability of signal-receiving cells to selectively sense and respond to a specific signal [3]. In contrast, traditional models predict that the signal presentation from the source via free secretion and extracellular diffusion is an unbiased non-selective process. However, recent advances in microscopy revealed that both signal-producing and receiving cells could extend signaling filopodia named cytonemes and selectively deliver or receive signals through cytoneme-cell contact sites [4–9]. Essential roles of cytonemes or cytoneme-like filopodia have been discovered in many vertebrate and invertebrate systems and are implicated in most signaling pathways, including Hh, Dpp, FGF, EGF, Ephrin, and Wnt under various contexts [4–19]. The prevalence and similarities of these signaling filopodia suggest that the polarized target-specific morphogen exchange through filopodial contacts is an evolutionarily conserved signaling mechanism.

These findings bring along a paradox - not only do signals instruct cells and organize discrete cellular patterns, but cells also control the spatiotemporal patterns of signal presentation and reception by organizing the distribution of cytonemes and cytoneme contacts [6,9]. The functioning of this interdependent relationship of signals and signaling cells through cytonemes, however, would require precise spatiotemporal coordination between cytoneme contact formation and signal release. We started the current investigation with the premise that a better understanding of the processes that produce cytoneme contacts and control contact-driven signal release is essential to understanding morphogenesis. We asked: (1) How do cytonemes recognize a specific target cell and form signaling contacts? (2) How are secreted signals controlled for polarized target-specific release, exclusively at the cytoneme contact sites? (3) Do cytoneme contact formation and signal release spatiotemporally coordinate with each other? If so, how?

To address these questions, we focused on the inter-organ dispersion of a *Drosophila* FGF, Branchless (Bnl), during the development of the wing imaginal disc-associated air-sac primordium (ASP) [20,21]. Bnl is expressed in a discrete group of wing disc cells, and it induces morphogenesis of the tubular ASP epithelium that expresses the Bnl receptor, Breathless (FGFR/Btl) [9,20,22]. Epithelial cells at the ASP tip extend polarized Btl-containing cytonemes to contact Bnl-producing wing disc cells and directly take up Bnl in a contact- and receptor-dependent manner [5,9]. The formation of Bnl-specific polarity and contacts of ASP cytonemes are self-sustained by Bnl-signaling feedbacks [9]. Consequently, Bnl reception via cytonemes can precisely sense and adapt to dynamic changes in coordination with ASP growth. With increasing distance from the Bnl-source, ASP cells extend gradually fewer polarized Bnl-receiving cytonemes, leading to the emergence of asymmetric Bnl dispersion and signaling patterns within the ASP [9]. However, how ASP cytonemes might recognize the *bnl*-source for signaling contacts, and, on the other hand, how Bnl producing cells might both inhibit random Bnl secretion and facilitate Bnl release selectively at the cytoneme contact sites are unknown.

Here, we discovered that Bnl is post-translationally lipid-modified by the addition of a glycosylphosphatidylinositol (GPI) moiety, which anchors Bnl to the outer leaflet of its source cell membrane and selectively presents Bnl to only Btl-expressing cells in an asymmetric manner. We provide evidence that the GPI-anchored Bnl on the source membrane can bind to Btl on the recipient cell membrane and, like cell adhesion molecules (CAMs) [23–29], induce contact-dependent adhesion and bidirectional Btl-Bnl signaling between the source and recipient cells. We further characterized how this CAM-like bidirectional signaling enables the source and recipient cells to coordinate with each other over distance and reciprocally promote each other to project cytonemes to establish contacts. Moreover, although the GPI anchor inhibits free/random Bnl secretion, it facilitates the release of Bnl exclusively at the cytoneme contact sites, ensuring its tissue-specific morphogen-like dispersion and signaling patterns. Thus, lipidation enables Bnl to spatially organize target-specific cytoneme contacts for its tissue-specific release. These findings suggest that while cytonemes are critical for organizing Bnl signaling patterns, the GPI-anchored Bnl programs the distribution of cytonemes to self-regulate its dispersion.

Results

Bnl presentation and reception reciprocally polarize each other by cytonemes.

Bnl is produced in the wing disc and transported target-specifically to the overlaying ASP via Btl-containing ASP cytonemes across a layer of interspersed myoblasts (Fig. 1A,B) [9]. The *bnl*-specific polarity of ASP cytonemes might be determined by the extrinsic patterns of Bnl presentation from the source. Previously, a non-permeabilized anti-Bnl immunostaining (αBnl^{ex}) designed to detect secreted externalized Bnl (Bnl^{ex}) [9,30] showed that the Bnl^{ex} was not randomly dispersed in the source-surrounding extracellular space (Fig 1A). Instead, Bnl^{ex} was restricted exclusively to the basal surface of Bnl-producing cells and on the ASP cytonemes. Importantly, even within the *bnl*-expressing disc area, Bnl^{ex} puncta were asymmetrically congregated near the contact sites of Btl-containing ASP cytonemes that received Bnl^{ex} (Fig. 1A,C). These results indicated that the Bnl presentation on its source surface is likely to be spatially polarized.

To examine if Bnl distribution in source cells is spatially biased toward the ASP, we co-expressed Bnl:GFP with mCherryCAAX (prenylated mCherry for membrane marking) under *bnl-Gal4*. Strikingly, although *bnl-Gal4*-driven mCherryCAAX equally labeled all source cells, Bnl:GFP was asymmetrically enriched at the ASP-proximal source area

(Figs.1D-D''; S1A,A'). Bnl:GFP puncta were also displayed on short polarized cytonemes emanating from the ASP-proximal disc cells (Figs.1D; S1A). To further verify if the Bnl presentation is polarized via cytonemes, we imaged the distribution of endogenous Bnl:GFP^{endo}, expressed from a *bnl:gfp*^{endo} knock-in allele [9], in the mCherryCAAX-marked *bnl*-source. Bnl:GFP^{endo} puncta represented all Bnl isoforms. Indeed, Bnl:GFP^{endo} puncta were selectively enriched in source cell cytonemes that oriented toward the ASP (Figs.1E,E'; S1B).

To thoroughly examine the organization of Bnl-presenting source cytonemes, we detected source cytonemes in unfixed wing discs that expressed a fluorescent membrane marker (e.g., CD8:GFP or CherryCAAX) either in all of the *bnl*-expressing cells (Fig. 1F,G) or in small clones of cells within the Bnl-expressing area (see Methods; Fig. 1H-H''). Three-dimensional image projections of live discs revealed that each of the Bnl-expressing columnar cells proximal to the ASP extended ~2-4 short (<15 μm) cytonemes perpendicularly from their basal surface (Figs. 1F-H''; S1A-D; Movie S1). The organization of source cells therefore can be described as polarized for Bnl presentation with basal cytonemes extending toward the ASP or ASP cytonemes. This organization is mirrored in the ASP, which is known to exhibit polarized Btl synthesis/localization, Bnl reception, and cytoneme orientation toward source cells [9]. Thus, the cellular components responsible for Bnl presentation in the disc source and for its reception in the ASP are likely to be reciprocally polarized toward each other.

Reciprocal guidance of Bnl-delivering and -receiving cytonemes.

To examine if Bnl-sending and -receiving cytonemes could reciprocally promote each other's polarity, we examined live wing discs harboring the CD8:GFP-marked ASP and mCherryCAAX-marked source. Time-lapse imaging of ex vivo cultured discs revealed that ASP and source cytonemes orient toward each other, and transiently contact each other's tips, bases, or shafts as they dynamically extend and retract (Fig. 1I-K''; Movie S2). Both cytoneme types had short lifetimes and repeated cycles of contact association-dissociation (S1E-H; Movies S2; Table S1). We also examined the inter-cytoneme interactions during different developmental stages. The ASP begins to develop during the early L3 larval stage, and it grows toward the disc *bnl*-source during the mid and late L3 stages to form the tubular ASP [20]. Despite the dynamic change in position of the ASP and disc *bnl*-source, their relative locations and the inter-cytoneme interactions at the ASP:source interface were maintained throughout larval development (Fig. S1I-L"). These results are consistent with the maintenance of a convergently polarized cytoneme-forming niche at the ASP:source interface.

Based on our previous results on cytoneme-mediated Bnl uptake in the ASP [5,9], Bnl is likely to be exchanged at the inter-cytoneme contact sites. However, it was technically challenging to visualize Bnl exchange during the dynamic inter-cytoneme interactions. Therefore, we sought to genetically ablate source cytonemes in *bnl:gfp*^{endo} larvae and analyze if the levels of Bnl:GFP^{endo} uptake in the ASP is reduced. An actin modulator formin, Diaphanous (Dia) could influence source cytonemes. Overexpression of Dia:GFP or a constitutively active Dia:GFP^{ca} induced cytonemes (Fig. 2A-E). Asymmetric enrichment of Dia:GFP^{ca} puncta in source cytoneme tips suggested localized Dia activity (Fig. 2C). In contrast, *dia* knockdown (*dia-i*) in the mCherryCAAX-marked source (*bnl-Gal4 x UAS-dia-i,UAS-mCherryCAAX*) suppressed cytoneme formation without any visible effects in *bnl* expression (Figs. 2A-E, S2A). Importantly, the *dia-i* mediated ablation of source cytonemes in *bnl:gfp*^{endo} larvae significantly reduced Bnl:GFP^{endo} uptake in the ASP. These ASPs were abnormally stunted, suggesting a reduction in Bnl signaling (Fig. 2F-H). Thus, source cytonemes are required to deliver Bnl to the ASP.

Inter-cytoneme Bnl exchange is consistent with reports that Hh and Wg are both sent and received by cytonemes[10,31,32]. However, how do source and ASP cytonemes find and adhere to each other over distance? Dynamic interactions of Bnl-exchanging cytonemes that are convergently polarized toward each other suggested a possibility of contact-dependent reciprocal guidance of source and recipient cytonemes. To test this possibility, we first ablated source cytonemes by *dia-i* expression and analyzed the non-autonomous effects on CD2:GFP-marked ASP cytonemes. The ablation of source significantly reduced the long, polarized ASP tip cytonemes (Fig. 2I-K). In contrast, short, randomly oriented ASP cytonemes were unaffected. Thus, Bnl-presenting cytonemes are required for the formation of the polarized Bnl-receiving ASP cytonemes.

We next removed ASP cytonemes by expressing *dia-i* under *btl-Gal4* and recorded non-autonomous effects on mCherryCAAX-marked source cytonemes. To avoid lethality, *dia-i* expression had to be controlled with Gal80^{ts} (see Methods). Tracheal *dia-i* expression not only reduced ASP cytonemes but also non-autonomously reduced source cytonemes (Fig. 2L-N'). Similarly, tracheal expression of a dominant-negative form of Btl (Btl-DN) was known to suppress ASP growth and cytoneme formation, without affecting the wing disc development [20]. When both source and Btl-DN-expressing tracheal cells were marked, the complete loss of ASP and ASP cytonemes was found to produce a corresponding loss of *bnl*-source cytonemes (Fig. 2O,P). Thus, Btl-presenting ASP cytonemes are required to produce source cytonemes that polarize toward the ASP. Collectively, these results suggested that the source and recipient cytonemes reciprocally guide each other to form signaling contacts.

CAM-like Btl-Bnl binding drives bidirectional contact matchmaking of cytonemes. The above results also suggested that the inter-cytoneme interactions might recruit and activate a bidirectional signaling mechanism, responses of which could induce ASP cells to extend Btl-containing cytonemes toward the source and activate source cells to extend Bnl-containing cytonemes toward the ASP. We hypothesized that such selective matchmaking between source and ASP cytonemes could be mediated by the binding of surface displayed Btl and Bnl. In this model, Btl and Bnl are analogous to cell-recognition or cell-adhesion molecules (CAMs), physical interaction of which can produce selective cell-cell adhesion and contact-mediated bidirectional signaling [24,33,34]. The initiation of such CAM-like interactions might not require Btl activation for canonical transcriptional outputs [35]. An alternative possibility is that the Bnl-Btl binding activates MAPK signaling and transcription of target genes in the ASP, and these gene products, in turn, non-autonomously act on the wing disc *bnl*-source to induce a response.

Notably, Btl:DN can bind to Bnl via its extracellular ligand-binding domain (see supplemental Fig. S2B) and can heterodimerize with *WT* Btl, but cannot activate nuclear MAPK signaling due to the lack of its intracellular kinase domain [20,22]. As observed before [13,20], while most wing discs with Btl:DN-expressing trachea (TC) had completely suppressed ASP/ASP cytonemes, occasionally the condition could produce partially suppressed nascent ASP-like growth with a range of variable numbers of ASP cytonemes orienting toward the source. Strikingly, in each of these discs, the appearance of polarized ASP cytonemes correlated with the concomitant appearance of similar numbers of polarized source cytonemes, forming direct cytoneme:cytoneme adhesive contacts (Fig. 3A-C). These results were consistent with the idea that source and ASP cells reciprocally promote each other's cytoneme-forming polarity via contacts. Such reciprocal contact-dependent interactions apparently were mediated by the Btl:DN-Bnl binding at the contact sites. Non-permeabilized αBnl^{ex} staining showed that Bnl^{ex} was selectively enriched at these inter-cytoneme contact sites (Figs. 3D,D', S2C-C'''). Similarly, when we expressed Btl:DN:Cherry in trachea, ASP cytonemes colocalized Btl:DN:Cherry puncta with Bnl^{ex} (Figs. 3E,E'; S2D,D'). Thus, Btl:DN on the ASP cytonemes could bind to Bnl^{ex} presented on the source membrane, and, despite the lack of its intracellular kinase domain, apparently could initiate a reciprocal contact-dependent matchmaking process. This result provided a clue that the Btl-Bnl binding might be critical for the inter-cytoneme contacts.

To further verify if the intercellular adhesive interactions were due to the CAM-like Btl-Bnl binding, we used an in vitro cell culture-based assay using *Drosophila* S2 cells (embryonic hemocyte lineage) to recapitulate cell-cell adhesion. S2 cells lack endogenous Btl and Bnl expression (modENCODE expression data), but when S2 cells ectopically expressed Bnl, αBnl^{ex} immunostaining detected enrichment of Bnl^{ex} on the expressing cell surface similar to what was found on the wing disc Bnl source (Fig. S2E,E'). Moreover, the lack of polarity and cell junctions in S2 cells was another suitable feature for ectopic induction of cell adhesion. As illustrated in Figure 3F, we mixed and co-incubated Bnl:GFP-expressing cells (S2-Bnl:GFP) with cells that expressed either

Btl:Cherry (S2-Btl:Cherry), Btl-DN:Cherry (S2-Btl:DN:Cherry), or a secreted sBtl:Cherry that lacked transmembrane and intracellular domains (S2-sBtl:Cherry).

Strikingly, S2-Bnl:GFP cells selectively adhered to both S2-Btl:Cherry and S2-Btl-DN:Cherry cells by forming trans-synaptic receptor-ligand co-clusters (Figs. 3G-M'; S2F-H, Movie S3). However, S2-Bnl:GFP cells failed to adhere to S2-sBtl:Cherry cells (Figs. 3H,N; S2G-J'). The selective adherence of Bnl-expressing cells with Btl- or Btl:DN-expressing cells and the correlation of the cell-cell adhesion with the occurrence of the trans-paired co-clustered organization of Btl and Bnl at the contact interfaces suggested that the Btl-Bnl binding could produce selective cell-cell adhesion. This process was reminiscent of receptor-ligand-dependent formation of immunological synapses [36]. We also observed localized enrichment of f-actin (phalloidin-stained) at the synaptic interface (Movies S3, S4, S5). Apparently, the components for Bnl delivery and reception reciprocally polarized toward each other at the cell-cell contact sites.

Non-transfected S2 cells and S2-Btl:Cherry alone rarely (average ~2-5% of cells) had nuclear dpERK a probe for canonical MAPK/FGF signaling (Fig. 3J,J'). Similarly, co-cultured S2-sBtl:Cherry lacked nuclear dpERK (Figs. 3I; S2J,J'). In contrast, at least 98% of S2-Btl:Cherry that were trans-paired to S2-Bnl:GFP had nuclear localized dpERK. In the same experiment, most unpaired S2-Btl:Cherry cells lacked nuclear dpERK, even when they were localized near S2-Bnl:GFP cells (Figs. 3I,K,K'; S2I,I’). We considered this selective polarized induction of dpERK in the trans-paired recipient cells as a successful in vitro recapitulation of the contact-dependent asymmetric Btl-Bnl signaling [9]. Importantly, S2-Btl:DN:Cherry, although could not activate dpERK, showed highly efficient trans-pairing with S2-Bnl:GFP (Figs. 3H,I,L-M’; S2F,H). Since the nuclear activation of MAPK signaling was not required for Btl:DN::Bnl trans-pairing, we conclude that Btl and Btl:DN acted as CAMs to physically bind to the surface-bound Bnl, thereby inducing selective adherence of the receptor- and ligand-expressing cells.

Bnl is tethered to the source cell surface by a GPI anchor.

To drive CAM-like cell-cell adhesion, Bnl needs to be tightly associated to the source cell membrane. How might a secreted protein be associated exclusively on the source cell surface without being randomly dispersed in the extracellular space? A probable mechanism emerged while exploring post-translational Bnl modifications during its intracellular trafficking [37]. Previously, we showed that a small N-terminal portion (residue 1-164) upstream of the central 'FGF domain' of Bnl is cleaved off in the source cell Golgi by Furin1, and this process enhances polarized trafficking of the remaining C-terminal signaling portion of Bnl to the basal side of the source cell (Fig. 4A; [37]). Therefore, when cells expressed a Furin-sensor $HA_1Bnl:GFP_3$ construct with HA (site 1) and GFP (site 3) flanking the Furin cleavage site, the cleaved HA-tagged portion was retained in the Golgi and the truncated $Bnl:GFP_3$ fragment was externalized for dispersal [37]. These observations led to a hypothesis that cells expressing a triple-tagged $HA_1Bnl:GFP_3Cherry_c$ construct with a C-terminal mCherry fusion (Fig. 4A) would externalize a truncated $Bnl:GFP_3Cherry_c$ portion marked with both GFP and mCherry.

However, when we expressed $HA_1Bnl:GFP_3Cherry_c$ (hereafter called $Bnl:GFP_3Cherry_c$) in S2 cells, GFP and mCherry tags were separated, and, importantly, while the $Bnl:GFP_3$ portion was localized on the cell surface (detected with both GFP and αGFP^{ex} immunostaining), the C-terminal mCherry remained intracellular (Fig. 4B-B'''). Notably, the C-terminal mCherry tag did not alter the predicted topology and physico-chemical properties of Bnl (Supplemental data). In fact, when $Bnl:GFP_3Cherry_c$ was expressed in the wing disc source under *bnl-Gal4*, the mCherry was retained in source cells and the $Bnl:GFP_3$ portion was efficiently delivered to the ASP (Fig. 4C). These results indicated an intracellular $Bnl:GFP_3Cherry_c$ cleavage, which separated the C-terminal mCherry prior to the secretion of the truncated $Bnl:GFP_3$ portion. Cleavages at multiple locations in the Bnl backbone was consistent with the detection of multiple Bnl:GFP bands in Western blots of expressing cell lysates [37].

Bioinformatic analyses revealed that the Bnl C-terminus has a short 20 amino acid hydrophobic tail preceded by a hydrophilic spacer (Fig. 4A,A'). A 15-20 residue long hydrophobic C-terminal tail together with an immediately upstream hydrophilic spacer commonly constitutes the signal sequence (SS) of a pro-GPI-anchored protein (pro-GPI-APs) [26,38–40]. The C-terminal hydrophobic portion of the SS is cleaved off and replaced with a GPI moiety via a transamidation reaction in the endoplasmic reticulum (ER). GPI-APs are then trafficked to the cell surface and anchored to the outer leaflet of the plasma membrane by the phosphatidylinositol (PI) portion of the GPI moiety [26,38,39] (Fig. 4D). Because the presence of C-terminal tags does not prevent glypiation of pro-GPI-APs [39], we surmised that GPI-anchoring of Bnl might explain the intracellular cleavage of mCherry from Bnl:GFP$_3$Cherry$_c$ prior to the surface display of its truncated Bnl:GFP$_3$ portion.

To detect Bnl glypiation, we followed a standard phosphoinositide phospholipase C (PI-PLC)-dependent shedding assay using S2 cells. Since PI-PLC specifically cleaves the GPI moiety, PI-PLC-dependent shedding of a cell surface protein confirms GPI anchoring. However, the lack of PI-PLC-dependent shedding is not always due to the lack of a GPI anchor, as there are PI-PLC-resistant GPI moiety [41]. Using the *Gal4/UAS*-based system in S2 cells, we ectopically expressed GFP-GPI [42] (a positive control), untagged Bnl (co-transfected with CD8:GFP to detect transfection and expression), Bnl:GFP$_3$, HA$_1$Bnl:GFP$_3$ (henceforth referred as Bnl:GFP), and a palmitoylated cell-surface protein, the constitutively active *Drosophila* EGF, cSpitz:GFP [43] (a negative control). The levels of surface-bound proteins in cultured cells with and without PI-PLC treatment were probed with non-permeabilized αGFP^{ex} or αBnl^{ex} (for untagged Bnl) staining. We compared the ratio of the surface-localized immunoprobed proteins to the total protein per cell between conditions (see Methods). PI-PLC treatment induced shedding of source-surface Bnl^{ex}, and Bnl:GFP^{ex}, like a GPI-GFP control, but not of surface-bound cSpitz:GFP^{ex} (Figs. 4D,D',F, S3A-E). Thus, Bnl is a GPI-AP.

An in-silico analysis (Methods) predicted Bnl-S^{741} as a probable glypiation site (ω-site). Therefore, to verify if Bnl's C-terminal region acts as a SS, we generated - (i) Bnl:GFPΔC, lacking the C-terminal 40 amino acid residues including the putative ω site; (ii) Bnl:GFPΔC-TM, where the trans-membrane domain from the mammalian CD8a was added to the C-terminus of Bnl:GFPΔC; (iii) Bnl:GFP-ω^m, Bnl:GFP with mutated

ω, $\omega+1$, and $\omega+2$ sites; and (iv) bGFP-GPI, a secreted super-folder GFP (secGFP [9]) fused to Bnl's C-terminal 53 amino acids region (see Methods) (Fig. 4E). Bnl:GFPΔC and Bnl:GFP-ω^m were not localized on the producing cell surface, even without the PI-PLC treatment (Figs. 4D',G; S3F,H,I). However, when a TM domain was added to Bnl:GFPΔC (i.e., Bnl:GFPΔC-TM), the protein was surface localized in a PI-PLC-resistant manner (Figs. 4D-F; S3G,H).

Usually, readily secreted secGFP was not detectable on the expressing S2 cell surface (Fig. S3J,J'), but when the same secGFP was added with Bnl's SS to make bGFP-GPI, it showed PI-PLC-sensitive surface-localization (Fig. 4D-F). Thus, Bnl's SS is required for glypiation. Secreted Bnl can bind to GPI-anchored glypicans, and the binding site occurs at its conserved FGF domain (Fig. 4A) [44]. Therefore, we examined if PIPLC-dependent removal of surface Bnl could be due to the removal of Bnl-bound cell surface glypicans. We generated a Bnl:GFP$^{\Delta FGF}$ construct, where only the core 'FGF domain' was replaced with the sfGFP sequence keeping all other Bnl regions intact. This chimeric protein showed clear PIPLC-sensitive surface localization (Figs. 4E; S3K), indicating that the PIPLC acts directly on the GPI-anchored Bnl.

The GPI-AP signal sequences (including ω-sites) are known to have little sequence conservation, and its extreme C-terminal positioning is not an absolute requirement [40,45]. The Bnl constructs described here, were derived from the well-characterized *bnl-PA* isoform [21] that has been used in all previous reports of ectopic Bnl expression. Bnl also has a shorter splice variant (PC) (FlyBase) with altered C-terminal hydrophobicity (Fig. S4A-A'''). Therefore, we generated a Bnl:GFP-PC construct (Methods) and expressed it in S2 cells. PI-PLC treatment of S2 cells expressing Bnl:GFP-PC removed the surface-localized Bnl:GFP-PC, indicating its GPI-anchored display (Fig. S4B-G). Thus, both Bnl-PC and Bnl-PA isoforms are glypiated, but strikingly, with two distinct signal sequences.

Next, to detect Bnl's GPI-anchoring in vivo, we developed a PI-PLC assay on live ex vivo cultured wing discs (see Methods). First, we detected native extracellular Bnl by non-permeabilized immunostaining of ex vivo cultured w^- wing discs with a Bnl antibody that detects all Bnl isoforms (Fig. S4A,A'). Bnl^{ex} that normally was asymmetrically enriched on the disc source without PI-PLC treatment was significantly reduced with PI-PLC treatment (Fig. 5A-C). When Bnl, Bnl:GFP, Bnl:GFPΔC-TM, Bnl:GFPΔC, and Bnl:GFP-ω^{m} constructs were expressed under *bnl-Gal4*, PI-PLC treatment significantly reduced Bnl^{ex} and $\mathrm{Bnl{:}GFP}^{ex}$ on the source surface, but not $\mathrm{Bnl{:}GFP\Delta C\text{-}TM}^{ex}$ (Fig. 5D-M). As observed in S2 cells, $\mathrm{Bnl{:}GFP\Delta C}^{ex}$ and $\mathrm{Bnl{:}GFP}^{ex}\text{-}\omega^{m}$ puncta were not detected on source cells irrespective of the PI-PLC treatment (Figs. 5I,J,M; S5A-B).

Although $\mathrm{Bnl{:}GFP\Delta C}^{ex}$ was absent from the source membrane, it was broadly spread through the extracellular disc areas surrounding the source and was also received by the ASP, suggesting that the protein was readily secreted and randomly dispersed from the source (Fig. S5A,A'). Externalized $\mathrm{Bnl{:}GFP\Delta C}^{ex}$ contains the conserved glypican binding FGF domain, yet it was absent on the source surface, indicating that the secreted $\mathrm{Bnl{:}GFP\Delta C}^{ex}$ (or Bnl^{ex}) was not restricted on the source by glypican binding. However, restricted dispersion of $\mathrm{Bnl{:}GFP\Delta C}^{ex}$ might be possible outside the *bnl*-expressing area. In contrast, *bnl-Gal4*-driven Bnl:GFP-ω^{m} showed severely reduced externalization and dispersion (Fig. S5B). This was consistent with previous reports of ER retention of the uncleaved pro-GPI-APs, in contrast to the normal trafficking of the same protein with deleted SS [46,47]. These results indicated that Bnl is cleaved at C terminus and added with a GPI moiety, which both facilitated Bnl externalization/surface display, and inhibited its free/random secretion.

GPI-anchored Bnl acts as a CAM to produce target-specific cytoneme contacts.

To test if GPI-anchored Bnl acts like a CAM, we employed the cell culture-based assay to compare the trans-pairing efficiency of S2-Btl:Cherry with either S2-Bnl:GFPΔC, S2-Bnl:GFPΔC-TM, or S2-Bnl:GFP (control). Similar to S2-Bnl:GFP, S2-Bnl:GFPΔC-TM cells selectively trans-adhered to S2-Btl:Cherry by forming the polarized Btl-Bnl co-cluster at the synaptic interface (Fig. 6B,C). In contrast, S2-Bnl:GFPΔC and S2-Btl:Cherry cells rarely showed trans-paring (~1% frequency of juxtaposition, but lacked polarized Btl-Bnl co-clustering at the synaptic interface; Fig. 6A,C). Thus, Bnl's membrane anchoring, irrespective of the nature of the anchor, was critical for heterotypic CAM-like bidirectional Btl-Bnl matchmaking.

We next examined the autocrine and paracrine signaling of Bnl:GFP variants in S2 cells. >90% of S2-Btl:Cherry cells co-transfected with either Bnl:GFP, Bnl:GFPΔC, or Bnl:GFPΔC-TM localized nuclear dpERK, indicating a similar level of autocrine activity of these signal variants (Table S3A; S5C). In co-cultured non-autonomous condition, Bnl:GFP selectively induced dpERK in ~91% of the trans-paired S2-Btl:Cherry, but only 5% of the unpaired S2-Btl:Cherry in the same culture had dpERK (Table S3B). In contrast, almost 85% of S2-Btl:Cherry that were adjacent to S2-Bnl:GFPΔC did not show dpERK (Figs. 6A; S5D; Table S3B). The majority of dpERK-positive S2-Btl:Cherry when co-cultured with S2-Bnl:GFPΔC, had unpredictable random locations (Table S3B). Importantly, Bnl:GFPΔC-TM, regained the ability to selectively activate signaling in the trans-paired S2-Btl:Cherry (Fig. 6B,C; Table S3B). These results suggested that Bnl:GFPΔC is capable of signaling, but its non-autonomous activity is random, unpredictable. Similarly, the rescue of selective adhesion and polarized signaling with Bnl:GFPΔC-TM suggested that the Bnl's CAM-like selective adhesion with recipient cells might be a pre-requisite for efficient signaling and its polarized, organized patterns.

Next, to test if CAM-like bidirectional Btl:Bnl interactions occur through cytonemes in vivo, we compared how GPI-modified (Bnl:GFP) and non-GPI-modified Bnl:GFP variants (TM and ΔC) affected source and ASP cytonemes. Despite the Bnl:GFP overexpression, both ASP and source cytonemes retained their reciprocal polarity toward each other (Figs. 6D-F; S6G). Increase in extension-retraction rates of ASP cytonemes in this condition suggested an increase in signaling activity in the ASP (Movie S6; Table S1). In contrast, overexpressed Bnl:GFPΔC significantly suppressed the formation of polarized cytonemes from both source and ASP cells (Figs. 6G-I; S6A,B,G). Short cytonemes, when detectable, lacked any directional bias and Bnl:GFPΔC localization.

Importantly, unlike Bnl:GFPΔC, Bnl:GFPΔC-TM strongly induced both ASP and source cells to extend large numbers of long polarized cytonemes that were stably adhered to each other via their tips and lateral sides (Figs. 6J-L; S6C-H; Movies S7-9). Bnl:GFPΔC-TM-exchanging cytonemes showed a significantly higher stability and longer contact lifetime than WT or Bnl:GFP-exchanging cytonemes (Figs. 7D,E; S6H; Movies S10,11; Table S1). Furthermore, Bnl:GFPΔC-TM puncta were populated at multiple inter-cytoneme contact interfaces (Figs. 6J,K; 7A-A''; S6E-F; Movies S7-9). The increase in the stability of inter-cytoneme contacts might account for an increase in the intensity of bidirectional responses with Bnl:GFPΔC-TM than with Bnl:GFP. To visualize the CAM-like heterophilic Bnl-Btl binding at the inter-cytoneme contacts, we expressed Bnl:GFPΔC-TM from the CD4:IFP_2-marked wing disc source in *btl:cherry^{endo}* larvae. These larvae expressed endogenous Btl:Cherry^{endo} in the ASP. Btl:Cherry^{endo} puncta on the ASP cytonemes were co-clustered with Bnl:GFPΔC-TM puncta at multiple contact sites along the length of the source and recipient cytonemes (Fig. 7B-C). Collectively, these results support the CAM-like bidirectional Btl:Bnl interactions through cytonemes.

To further verify reciprocal induction of cytonemes by bidirectional Btl:Bnl interactions, we induced ectopic Bnl:GFPΔC-TM expression from randomly-localized mCherryCAAX-marked wing disc clones (Methods) and examined if the ectopic source cells could polarize cytonemes toward the ASP (Fig. 7F-J). Clones in the wing disc pouch that were far away from the ASP did not establish contact with the ASP and only had short randomly oriented signal-containing cytonemes (Fig. 7F,G,H). In contrast, ectopic clones in the disc notum, proximal to the ASP, extended long polarized cytonemes contacting the ASP (Fig. 7F,I,J). These results are consistent with the idea of contact-dependent retrograde signaling response in the Bnl source, reinforcing cytoneme polarity and contacts. Similarly, ASP cells extend cytonemes toward ectopic Bnl-expressing clones [20] and the source-specific polarity is reinforced by Bnl signaling feedback [9]. When we ectopically expressed Btl:GFP in randomly-localized clones of wing disc cells, Btl:GFP-expressing disc clones and the mCherryCAAX-marked Bnl-source were found to extend polarized cytonemes toward each other (Fig. 7K-M'). These results suggested that CAM-like bidirectional Bnl:Btl signaling can be adaptive and can organize context-specific spatial patterns of the source and recipient cytonemes.

Bnl's GPI anchor ensures contact-dependent tissue-specific Bnl release.

Although Bnl:GFPΔC-TM induced strong bidirectional responses that were manifested in cytoneme polarity and inter-cytoneme contacts, Bnl:GFPΔC-TM-exchanging cytonemes had a significantly longer lifetime than WT or Bnl:GFP-exchanging cytonemes (Figs. 7D,E; S6H; Table S1). Moreover, unlike Bnl:GFP, Bnl:GFPΔC-TM puncta were often abnormally internalized into the ASP with colocalized source cell membrane, indicating a defect in release of the TM-tethered signal from the source cell membrane (Figs. 8A,D,E; S7A-C'; Movie S14). When both source and ASP cells were simultaneously marked and imaged in time-lapse, Bnl:GFPΔC-TM-exchanging cytonemes appeared to resist contact dissociation, leading to cytoneme breakage and absorption of the source membrane in the ASP (Movies S11). We predicted that GPI anchoring might be critical for efficient tissue-specific Bnl release and cytoneme contact-dissociation.

To investigate if GPI-anchoring of Bnl facilitates its target-specific release, we compared the spatial distribution of GPI-modified (Bnl:GFP) and non-GPI-modified Bnl:GFP constructs (ΔC and TM) expressed from the mCherryCAAX-marked wing disc Bnl source. As observed before [9,37], despite overexpression in the disc *bnl*-source, Bnl:GFP puncta were not randomly spread in the non-expressing disc areas, but were exclusively transferred to the ASP (Fig. 8A; Movie S12). In contrast, two ΔC variants (Bnl:GFPΔC and Bnl:GFPΔC_{168}), showed dispersion in the non-specific disc areas surrounding the source (Fig. 8B,C; Movie S13). Importantly, the corresponding Bnl:GFPΔC-TM and Bnl:GFPΔC_{168}-TM variants regained the exclusive ASP-specific distribution, but their range of distribution was restricted only to the ASP tip, indicating reduced levels of signal exchange (Figs. 8D,E; S7A-C'; Movie S14). These results suggested that GPI anchoring might be required for both inhibiting free/random Bnl secretion/dispersion and activating target-specific contact-dependent Bnl release.

To better examine such dual roles of GPI anchoring, we compared the ASP-specific and non-specific spread of different Bnl:GFP variants over time in live ex vivo cultured discs (see Methods). To accurately probe and estimate the levels of signal uptake in the ASP, we took advantage of the dual-tagged Furin-sensors - $HA_1Bnl:GFP_3$, $HA_1Bnl:GFP_3\Delta C$-TM, and $HA_1Bnl:GFP_3\Delta C$ (Fig. 8F-S). In normal and ex-vivo cultured larval discs, the N-terminal HA-tagged portion (αHA-probed) of all three constructs were cleaved in source cells and only their truncated $Bnl:GFP_3$ portions were transferred to the ASP (Fig. 8F,G,J,M). However, when Furin inhibitors were added to the culture media, uncleaved signals (αHA-probed) started to be received by the ASP[37]. Therefore, the ratio of levels of HA-probed uncleaved signal to the total GFP-probed signal (pre-existing $Bnl:GFP_3$+ $HA_1Bnl:GFP_3$) in the ASP during a Furin-inhibited period provided a semi-quantitative estimate of the rate of uptake of the signal (Fig. 8F').

As observed before [37], the levels of $HA_1Bnl:GFP_3$ (control) uptake in the ASP gradually increased with increasing duration of the culture. In comparison, the levels of $HA_1Bnl:GFP_3\Delta C$-TM and $HA_1Bnl:GFP_3\Delta C$ in the ASP did not change dramatically, indicating a slow rate of ASP-specific transfer of the variants (Fig. 8G-P). Notably, even after a 5 h of culture, $HA_1Bnl:GFP_3$ dispersed exclusively to the ASP (Fig. 8Q). In contrast, within a 5 h of incubation period, $HA_1Bnl:GFP_3\Delta C$ was randomly localized in the source-surrounding disc areas, but was barely received by the ASP from the same disc (Fig. 8J-L,Q-S). These results suggested that GPI anchoring is required to both inhibit free Bnl secretion/dispersion and activate its directed contact-dependent release.

Bnl's GPI-anchor is required for polarized spatial patterns of Bnl signaling.

To investigate if GPI anchoring and contact-dependent release is important for Bnl signaling, we generated small gain-of-function (GOF) clones expressing GPI-modified and non-GPI-modified Bnl:GFP variants directly within the ASP epithelium, as described earlier [9]. To distinguish the ectopically induced signaling patterns from the endogenous signaling patterns, we analyzed small (2-3 cell) clones within the ASP stalk and transverse connective (TC), which lack Bnl uptake from the original disc source and

MAPK signaling [9] (Fig. S7D). In consistence with earlier reports [9], all cells within a ~3 cell diameter area surrounding a Bnl:GFP GOF clone received Bnl:GFP, and all Bnl:GFP-receiving cells also induced dpERK (Fig. 9A,A',D; S7G). In comparison, Bnl:GFPΔC was received by many cells surrounding its clonal source, but only a few randomly located Bnl:GFPΔC-receiving cells induced dpERK (Figs. 9B,B',D; S7E,G). Apparently, the normal spatial correlation between the signal uptake and signaling was lost with Bnl:GFPΔC.

The spatial correlation between signal and signaling was regained with Bnl:GFPΔC-TM. However, Bnl:GFPΔC-TM activity was restricted to only a few juxtaposed cells close to the clonal source (Figs. 9C,D; S7F,G). Similarly, when either Bnl:GFP, Bnl:GFPΔC, or Bnl:GFPΔC-TM was overexpressed from the disc *bnl*-source under *bnl-Gal4*, unlike Bnl:GFP or Bnl:GFPΔC-TM, a significant number of Bnl:GFPΔC-receiving ASP cells lacked nuclear MAPK signaling (Figs. 9D; S7H-L). These results suggested that the GPI anchoring and contact-dependent Bnl release are likely required for the normal coordination between signal dispersion and interpretation.

Bnl's activity was also assessed by its ability to chemoattract tracheal branches. Bnl was known to induce chemotactic migration of tracheal branches toward its ectopic point source [48,49]. Therefore, we ectopically expressed the GPI-modified and non-GPI-modified Bnl:GFP variants at equivalent levels in a non-essential organ, the larval salivary gland [37,49]. Since wild-type salivary glands are completely devoid of tracheal connections and *btl* or *bnl* expression, the extent of new tracheal connection produced in the salivary glands due to the ectopic Bnl expression provided an unbiased estimate of Bnl signaling outcome [37,49].

Strikingly, while Bnl:GFP and Bnl:GFPΔC-TM induced extensive tracheal invasion and branching into the expressing salivary gland, Bnl:GFPΔC did not (Fig. 9E-H). We predicted that the extent of tracheal invasion/branching might be correlated with the levels of Bnl retention on the source cell surface. Indeed, the level of Bnl:GFPΔC on the salivary gland surface relative to its total expression was significantly less than that of Bnl:GFP or Bnl:GFPΔC-TM (Fig. 9I-L). Thus, although Bnl:GFPΔC can activate receptors (Fig. S5C, Table S3), its unavailability on the source cell surface caused the loss of its ability to guide tracheal branching into its source. In contrast, the same signal, when was tethered to the source membrane by a TM domain (Bnl:GFPΔC-TM), it regained the normal chemotactic function for tracheal invasion. These results suggested that Bnl retention on the source surface is critical for tissue-specific signaling patterns.

DISCUSSION

This study uncovered an elegant program of reciprocal inter-organ communication that is encoded by the lipid-modification of FGF/Bnl and orchestrated by its cytoneme-mediated contact-dependent signaling. It provided insights into how cytonemes select a specific target to establish signaling contacts, exchange signals at their contact sites, and dynamically inform cells where they are, what they should do, and when (Fig.10). Furthermore, it also discovered the first lipid-modified FGF and characterized how lipidation enables the signal to program these cytoneme-mediated cellular events to self-regulate its diverse context-specific dispersion and interpretation patterns.

We discovered that Bnl is GPI anchored to the source cell surface, and this modification facilitates the signal to simultaneously act as a local CAM and a long-range paracrine morphogen/growth factor. Mechanistically, GPI-anchored Bnl directs three cellular events: cytoneme-mediated target selection, target-specific signal release, and feedback regulations of these processes (Fig. 10). We showed that GPI-anchored Bnl on the source cell surface and Btl on the receiving cell surface act as heterophilic CAMs. Bnl source and recipient cells extend cytonemes to present Bnl and Btl on their surfaces, and when Btl-Bnl binding occurs, it leads to selective cell-cell cytoneme contact formation over distance. The CAM-like Btl-Bnl binding induces forward signaling in the ASP and retrograde signaling in the source, feedback responses of which promote these cells to reinforce the reciprocal polarity of Bnl-receiving and Bnl-sending cytonemes toward each other. This explains how the CAM-like bidirectional Btl-Bnl signaling can drive the reciprocal guidance of the source and ASP cytonemes.

Traditionally, most secreted signals are envisioned to orchestrate morphogenesis unidirectionally, only in recipient cells, and induce morphogenesis by activating cascades of target genes, which, in turn, control functions. In contrast to this general idea, lipidated Bnl physically regulates the polarity and interactions of signaling cells/cytonemes and induces contact-dependent bidirectional Bnl-Btl signaling to control both source and recipient cells. Elegantly, the cause and effect of this signaling process can control each other and, consequently, produce a wide range of interdependent functions by using only a few basic molecular/cellular steps. For instance, the same cytoneme contacts that the Btl-Bnl binding helps to form also bring Btl and Bnl molecules together to interact. Thus, not only is the signal exchange cytoneme/contact-dependent, but the cytoneme contacts are also formed signal- or tissue-specifically. Similarly, Bnl and Btl each can simultaneously act as both a ligand and a receptor for the other. In this regard, cytonemes play an important role in physically integrating various functions in time and space through their contact sites.

This bidirectional signaling mechanism for cytoneme contact formation is reminiscent of CAM-mediated bidirectional pre-synaptic and post-synaptic filopodial matchmaking that organizes *Drosophila* neuromuscular junctions [33]. Bidirectional transmission of information is the basis for neuronal synaptic assembly, plasticity, and functions, suggesting probable conservation of this basic signaling strategy in all cells. We propose that by employing the contact-mediated Btl-Bnl bidirectional signaling through cytonemes, source and ASP cells can inform each other of their relative locations, directionality, and signaling activity over distance and reciprocally coordinate with each other to sculpt context-specific self-organized architectures. This contact-dependent bidirectional signaling might also be the driving force of the dynamic reciprocal coordination and co-migration of embryonic *bnl*-sources and tracheal branches [50].

Secretion and dispersion of most paracrine signals like Bnl are required for long-range morphogen-like signaling. However, in this general paradigm, source surface retention is inhibitory to secretion and long-range spreading. In contrast, we found that the purpose of GPI anchoring is to release the Btl-bound Bnl specifically to the recipient cells/cytonemes and facilitate variable recipient-specific long-range dispersion and signaling patterns. This is consistent with our previous finding showing that the Bnl availability on the source surface controls the levels of cytoneme-dependent Bnl signaling in the ASP [9,37]. How signal retention might facilitate its recipient-specific long-range spread can be explained by our previous findings of self-generation of cytoneme-mediated signaling patterns by Bnl-signaling feedbacks [9,37].

Thus, GPI-anchored Bnl apparently provides a balance between two extreme functions - free/random secretion (e.g., morphogen-like function) and no secretion (e.g., CAM-like local organization). Our results suggest that this dual strategy of inhibition and activation of signal spread is responsible for different morphogenetic functions. For instance, Bnl's CAM-like activity is critical for tracheal chemotaxis as well as reciprocal adhesion and the polarized spatial organization of source and recipient cells. We propose that the Bnl's CAM-like selective activity is a prerequisite for its polarized release and asymmetric organization of morphogen-like signaling patterns. Consequently, although a readily secreted non-GPI Bnl can activate the receptor, it fails to mediate both CAM-like bidirectional and morphogen-like cell organizing functions. On the other hand, TM-tethered Bnl efficiently acts as a CAM but due to the poor release, causes a scaled-down patterning outcome.

Bnl release also dissolves the inter-cytoneme adhesive contacts. Dissociation of cytoneme:cytoneme contacts might be required for the context-specific adaptation of the emerging tracheal branches. Although Bnl release is critical for its normal functions, we do not know how Bnl is released and how the release mechanism is specifically activated at the cytoneme contact sites. Internalization of Bnl:GFP-∆C-TM puncta in the ASP together with the donor cell membrane indicated that Btl-bound Bnl is severed from its source surface prior to the receptor-mediated endocytosis. We speculate that an enzymatic shedding mechanism [51] might be activate at the cytoneme contacts.

The strategy of dual control of signal retention and selective dispersion might also be present in other signals. The *Drosophila* FGF, Pyramus (Pyr), is a transmembrane protein, and the TM-tethering is required for its spatiotemporal functions [52]. Ephrin-A and Ephrin-B are GPI- and TM-tethered proteins, and their membrane tethering causes bidirectional signaling [23]. Lipid modifications are known to be critical for the morphogenetic potency of Hh, Wnt, and EGF/Spi [43,53,54]. Analogous to Bnl, engineered TM-tethered forms of Hh, Spi, and Wnt can induce morphogenesis within a narrow range, and removal of lipid-modification of Hh, Spi, and Wnt causes unrestricted signal spreading but reduces their ability to organize tissues [43,55–59]. Moreover, all signals, including those that are not known to be lipidated (e.g., BMPs and many FGFs), can interact with GPI-anchored proteoglycans, which can restrict free signal dispersion and produce the biphasic activation and inhibition of signaling [60–62]. Glypicans also can control cytoneme-mediated communications [63–65]. Therefore, our findings showing how GPI anchoring enables Bnl to direct source and recipient cells to coordinate with each other by cytonemes provide important new insights into how various signal retention strategies might control signaling and morphogenesis.

METHODS

Fly genetics

Fly lines are described in Table S4. All flies were raised at 25 °C with a 12 h/12 h light/dark cycle, except tracheal *dia-RNAi* expression. All the experiments were performed under non-crowded situations. The sequence-verified DNA constructs were used to generate transgenic flies by P-element mediated germline transformation as described in Du et al [9]. Transgenic injections were performed by Rainbow Transgenic Flies, Inc.

Mosaic analyses

(i) To generate ectopic clones in the ASP*, hsFlp; btlenh>y+>Gal4,btlenh-mRFPmoe* females were crossed to males carrying *UAS-Bnl:GFP, UAS-Bnl:GFP⊿C, UAS-*

Bnl:GFP∆C-TM, or *UAS-Btl-DN.* Flip-out clones were generated by heat shocking early 3rd instar larvae at 37 □C for either 5 or 10 min. Larvae, then, were incubated at 25 □C until they reached the mid-late 3rd instar stages and dissected for further analysis.

(ii) To generate CD8:GFP-expressing clones in the *bnl* source, *hs-mFlp;bnlGal4* females were crossed to FlyBow *FB2.0* flies and clones were induced in the progenies by heat-shock as described in (i). Only CD8:GFP-marked cells were visualized in live tissues.

(iii) Ectopic Bnl:GFP-TM-expressing clones in the wing disc were induced in progenies of *hs-Flp;UAS-bnl:GFP-TM* (females) x *mCherryCAAX;act>CD2>Gal4* (males) cross.

iv) Ectopic Btl:GFP-expressing clones in the wing disc were induced in progenies of *hs-Flp;;UAS-Btl:GFP* (females) x *act>CD2>Gal4;;bnlLexA,LexO-mCherryCAAX* (males) cross.

Tissue-specific transgene expression

For the transgene expression in the trachea, *btl-Gal4/UAS* or *btl-LexA/LexO* systems were used. To express transgenes in the wing disc *bnl*-source, *bnl-Gal4/UAS* or *bnl-LexA/LexO* systems were used. The *bnl-Gal4/UAS* was also used to ectopically express Bnl:GFP variants in the larval salivary glands. Although *bnl* is not expressed in the salivary gland, *bnl-Gal4* is non-specifically expressed in the larval salivary gland [37].

Cytoneme removal from the ASP and *bnl*-source.

To remove source cytonemes, *UAS-dia-RNAi* was expressed under *bnlGal4* and larvae were reared at 25°C. In trachea, a high-level *dia-RNAi* expression (at 25°C) caused larval lethality. Therefore, *tub-*$Gal80^{ts}$; *UAS-diaRNAi* males were crossed to *btlGal4,UAS-CD8:GFP; bnlLexA,LexO-mCherryCAAX/TM6* females; The *btl-Gal4*-driven expression of *dia-RNAi* was suppressed by $Gal80^{ts}$ at 18°C until L3 stage and activated by shifting the temperature to 29°C (that inactivated $Gal80^{ts}$), 24 hr prior to harvesting the L3 larvae for imaging.

Cell lines and cell culture

Schneider's 2 (S2) cells were cultured and transfected following standard protocols described in Sohr et al [37]. Cells were transfected either with Lipofectamine 3000 or Mirus TransIT-Insect Transfection Reagent for CAM assays following manufacturer's protocol. Transient ectopic expression of various constructs in S2 cells was achieved by co-transfecting *act-Gal4* and *UAS-x* constructs (x = various cDNA or cDNA fusions) and analyzed after 48 hrs of incubation at 25°C.

Immunohistochemistry

The standard immunostaining and the extracellular immunostaining under live-cell non-permeabilized condition (αGFP^{ex} for GFP or αBnl^{ex} for Bnl) was carried out following protocols described in Du et al. and Sohr et al. [9,37]. Table S4 lists all antibodies used.

DNA constructs

All constructs used here are described in Table S4.

Bioinformatic analysis

DNA sequences were analyzed with SnapGene, Protein sequences were analyzed with MacVector, ProtScale (ExPASy), EMBOSS Pepinfo (www.ebi.ac.uk), PredGPI (http://gpcr.biocomp.unibo.it/predgpi).

Flow cytometric analyses

S2 cells expressing various constructs were immunostained and scanned using a BD CantoII (BD Biosciences) flow cytometer and the data were analyzed using FACSDiva (BD Biosciences). For quantitative assays as shown in Fig S3B-H, S4E-G, the number of cells detected in Q2 (GFP+ cells with αGFP^{ex}+) was divided by the number of cells in either Q2 or Q4 (total GFP+ cells) to obtain the Y-axis value. These values were obtained from three independent experimental repeats.

Ex vivo organ culture and Furin inhibition

Ex vivo wing disc culture, pharmacological inhibition of Furin in cultured discs, and analyses of ASP-specific uptake of Bnl were carried out following Sohr et al. [37,66]. The temporal increase in the levels of GFP-tagged Bnl in the ASP over time was difficult to assess due to the pre-existing Bnl:GFP$_3$ in the L3 ASP used for culturing. Therefore, we used Furin-sensors (HA$_1$Bnl:GFP$_3$, HA$_1$Bnl:GFP$_3\Delta$C-TM, and HA$_1$Bnl:GFP$_3\Delta$C) that were detectable by both αHA immunostaining and GFP. The time when tissues were transferred to the Furin-inhibited media, was considered as t=0 for the appearance of intact Furin sensors (HA$_1$Bnl:GFP$_3$). Tissues were incubated for 1, 2.5, and 5 hrs in the Furin-inhibited media, before harvesting for αHA immunostaining. For a comparative analyses among samples, we obtained a semi-quantitative estimate by measuring the ratio of the uncleaved sensor (αHA immunofluorescence intensity) to the total GFP signal (pre-existing Bnl:GFP$_3$ + post-inhibition HA$_1$Bnl:GFP$_3$) per ASP for t=1h or 2.5h or 5 h. For Fig. 8P, HA$_1$Bnl:GFP$_3$: n = 12 (1 h), 11 (2.5 h), 10 (5 h); HA$_1$Bnl:GFP$_3\Delta$C-TM: n = 16 (1 h), 18 (2.5 h), 15 (5 h); HA$_1$Bnl:GFP$_3\Delta$C: n = 8 (1 h), 14 (2.5 h), 11 (5 h). $p < 0.01$ for HA$_1$Bnl:GFP$_3$ vs HA$_1$Bnl:GFP$_3\Delta$C-TM or HA$_1$Bnl:GFP$_3\Delta$C at 2.5 h and 5 h.

CAM assay using S2 cells

~48 h post-transfection, S2 cells ectopically expressing either Btl variants (*UAS-Btl:Cherry*, *-BtlDN:Cherry*, or *-sBtl:Cherry*) or ligand variants (*UAS-Bnl:GFP* or *-Bnl:GFPΔC* or *-Bnl:GFPΔC-TM*) were resuspended in 1 ml of fresh M3 media. 200 μl of the receptor-expressing cells were gently mixed with 200 μl of the ligand-expressing cells for 10 min in a sterile tube. The well-mixed cell suspension was plated to the center of a sterile cover slip within a 6-well plate and incubated at 25^{o}C for 16 hrs before fixing them with 4% PFA following standard protocols. Coverslips were carefully mounted with cells facing down to 10 μl of the VECTASHIELD on microscopic slides. For comparative analyses, co-culture assays were performed in identical conditions. Cells were analyzed from more than three transfection repeats, with at least 30 random frames/experiment under 20X and 40X objectives. Regions with comparable cell density were analyzed. Adjacent cells with the ring-like heterophilic receptor-ligand co-clusters were considered as trans-paired cells and those without the receptor-ligand co-clusters were considered as juxtaposed. Homophilic Btl-Btl or Bnl-Bnl clusters between adjacent cells were rarely observed as indicated in Figure S2H. Cells were imaged in both 20X and 40X to thoroughly verify Btl-Bnl trans-pairing in the mixed cell population.

Autonomous and non-autonomous dpERK signaling in S2 cells

For autonomous MAPK signaling, S2 cells were co-transfected with *act-Gal4*, *UAS-Btl:Cherry,* and *UAS-X* (*X* = various Bnl:GFP variants) and prepared on cover-slips as described before. Cover slips with cells were processed with standard fixation and anti-dpERK immunostaining. The percentage of Btl:Cherry expressing cells with nuclear dpERK signals was scored with confocal microscope (20X/40X). For non-autonomous dpERK signaling, cells were prepared following the CAM assay, followed by PFA fixation and anti-dpERK staining. Both trans-paired and unpaired Btl:Cherry variants were recorded to estimate the contact-dependent non-autonomous dpERK signaling.

PIPLC treatment of wing imaginal discs and transfected S2 cells.

Transfected S2 cells (1 mL) were harvested (700 g, 5 min) in a 1.5 mL Eppendorf tube. Cells were washed twice in 1XPBS (500 µL each) and incubated either in 500 µL 1XPBS (control) or in PIPLC containing 1XPBS solution (1 U/mL PIPLC) at 20-25 □C for 30 min with gentle rotation. Cells were harvested and prepared for the standard non-permeabilized extracellular staining before imaging or FACS. To reliably compare the levels of surface-localized proteins with and without PIPLC treatment, the ratio of the surface:total Bnl levels per cell was measured using Fiji (at least 3 independent repeats). Note that the surface levels of GFP-tagged proteins per cell was measured with αGFP^{ex} immuno-fluorescence and the total GFP fluorescence of the same protein measured the total expression in the same cell. For untagged Bnl, CD8:GFP was co-transfected and the Bnl^{ex} level was normalized with CD8:GFP in the same cell.

For PIPLC assay in wing discs, third instar larvae were prepared following ex-vivo organ culture method [37] and transferred to 1.5 ml Eppendorf tubes containing 1 ml of either WM1 media (control) or WM1 media with PIPLC (1U/mL). Tissues were incubated for

30 min at 20-25^{o}C with gentle rotation. Then the PIPLC reaction was stopped by removing the solution and washing the tissues 3 times with WM1 media. Tissues were then prepared for extracellular staining as described before.

Live imaging of cytonemes

Wing imaginal discs were prepared and imaged in WM1 medium as described in Du et al. [9]. Time-lapse imaging of cytonemes was carried out in ex vivo cultured wing discs in Grace's insect culture medium as described in Barbosa and Kornberg (submitted). A spinning disc confocal microscope under 40X/60X magnifications were used to capture ~30-50 μm Z-sections with 0.2 μm step size of wing discs as described earlier [9]. For Fig. 1E,E', images were captured using the Zeiss LSM900 confocal with an Airyscan-2 detector in 60X magnifications. The images were processed and analyzed with Fiji. For 3D-rendering, Andor iQ3 and Imaris software were used.

Quantitative analyses of cytoneme number, orientation, and dynamics.

Cyonemes were manually counted and plotted by methods described in Du et al [9]. For ASP cytonemes, cytonemes were recorded across a 100 μm arc centered at the tip (Figs. 2I-K,L,M,M',N; 6D-L; S6G). Wing disc *bnl* source cytonemes were recorded from the 3D projections across a 100 μm perimeter surface centering at the ASP tip contact as a reference (Figs. 2A-E,L',M'',M''',N'; 6E-L; S6G). For Figure 2L',N', cytonemes were not grouped based on the length as all source cytonemes were less than 15 μm. For Figures 1L-N,7D-E, different parameters of cytoneme dynamics were measured following previous reports (see Table S1) [64,67].

Quantitative analyses of fluorescence intensities

The density of fluorescence intensity (e.g., spatial range and density of signals) was measured from maximum-intensity projections encompassing the relevant wing disc or ASP sections from a selected region of interest (ROI) using Fiji as described before [9]. For each genotype, at least 3 samples were used to obtain the average plot profile.

Sholl analysis for tracheation in salivary gland

The extent and frequency of tracheal branching on the larval salivary glands expressing Bnl:GFP, Bnl:GFPΔC-TM, or Bnl:GFPΔGPI was quantitated using Sholl analysis in Fiji as described in [37] .

Statistical analyses

Statistical analyses were performed using VassarStat and GraphPad Prism 8, MS Excel. P values were determined using the unpaired two-tailed t-test for pair-wise comparisons (Figs. 2H,K; 4F,G; 5C,F; S2A; S3A,H,K; S4D,G; Tables S1,S2), or the one-way ANOVA followed by Tukey's honestly significant different (HSD) test for comparison of multiple groups (Figs. 2E; 3H; 5M; 6C; 8P; 9D,H,L; S4I'; S6G). $p < 0.05$ is considered significant. The sample size (N) for each data analysis is indicated in the figures/figure legends/methods/source. Rose plots were generated by R software as described in [9].

RNA isolation and RT-PCR

Total RNA was extracted from 20 wing discs of the w^{1118} L3 larvae using TRI reagent (Sigma-Aldrich) followed by Direct-zol RNA purification kits (Zymo Research). Expression analyses of *bnl PA* and *PC* isoforms are described in Supplementary Information.

Acknowledgments

We thank Drs. T.B. Kornberg and G.O. Barbosa for sharing the design of the culture chamber for live imaging; Ge Yan, for R plot analyses; Drs. N. Andrews, T.B. Kornberg, W. Snell, and S. Ogden lab for comments on the manuscript; the Bloomington Stock Center for *Drosophila* lines; the DSHB for antibodies; A.E. Beaven for UMD imaging core facility. **Funding:** NIH grant R35GM124878 to SR. **Author Contributions:** A. Sohr discovered GPI-anchoring of Bnl and L. Du discovered its roles; S. Roy supervised the work and designed the project; L. Du, A. Sohr, Y. Li conducted experiments: S. Roy, L. Du, and A. Sohr wrote the paper. **Competing interests:** None declared.

Figure Legends

Fig. 1. Bnl presentation and reception reciprocally polarize each other via cytonemes. (A) Drawing depicting the organization of the ASP, wing disc, myoblasts, and Btl-containing ASP cytonemes receiving Bnl from the disc *bnl* source. **(B)** Spatial organization of the wing disc (*bnl-LexA,LexO-mCherryCAAX*) and ASP (*btlGal4,UAS-CD8:GFP*) cytonemes (arrow). **(C-E')** Polarized Bnl presentation from the source: (C) Externalized $\mathrm{Bnl}^{\mathrm{ex}}$ (red) on the source surface (dashed lined area); arrow, contact sites of Btl:GFP-containing ASP cytonemes (*btl:GFP* fTRG). (D-D') Wing disc expressing Bnl:GFP from mCherryCAAX-marked *bnl*-source cells (*UAS*-mCherryCAAX/+*; bnl-Gal4/ UAS*-Bnl:GFP). (D") Plot showing Bnl:GFP intensity profile within the boxed source area in D' along the proximal (p)-to-distal (d) direction (arrows) relative to the ASP (see Fig. S1A,A'). (E,E') Airyscan image of wing disc *bnl*-source extending $\mathrm{Bnl{:}GFP}^{\mathrm{endo}}$-containing cytonemes toward the ASP (*UAS*-mCherryCAAX/+*; bnl-Gal4/bnl:gfp*^{endo}). (D,D',E,E') dashed line, ASP; arrow, Bnl:GFP-presenting cytonemes; dashed arrow, endocytosed Bnl:GFP. **(F-H")** 3D-rendered images showing the ASP-specific polarity of source cytonemes; F,G, mCherryCAAX-marked source and nlsGFP-marked ASP (*btl-Gal4,UAS*-nlsGFP/+; *bnl-LexA,LexO*-mCherryCAAX/+); H,H', CD8:GFP-expressing clones within the *bnl* source area (see Methods); H", graphs showing the source cytoneme length distribution (see Fig. S1D). **(I-N)** Contact-dependent reciprocal guidance of source (red) and ASP (green) cytonemes (*btl-Gal4,UAS*-CD8:GFP/+; *bnl-LexA,LexO*-mCherryCAAX/+); arrowhead, contact site; J, illustration of I-K''; L-N, plots comparing ASP and source cytoneme dynamics as indicated (see Fig. S1E-H; Table S1). All, except C-E', live imaging. Scale bars, 20 µm; 5 µm (E,E',H,H').

Fig. 2. Bidirectional matchmaking of Bnl sending and receiving cytonemes for contacts. (A-E) 3D-rendered views of mCherryCAAX-marked *bnl*-source, showing autonomous effects of Dia:GFP, $\mathrm{Dia{:}GFP}^{\mathrm{CA}}$, and *diaRNAi* expression on source

cytoneme numbers (*UAS-mCherryCAAX;bnl-Gal4* X w^{-} for control, or *UAS-"*X"); A-D, arrow, source cytonemes, arrowhead, missing source cytonemes; E, graphs showing numerical values, as indicated. **(F-H)** Bnl:GFP^{endo} uptake in the ASP (dashed line) under control (*bnl:gfp*^{endo} X *bnl-Gal4*) and *dia-i*-induced source cytoneme-depleted conditions (*UAS-dia-i,bnl:gfp*^{endo} X *bnl-Gal4*); H, graphs showing numerical values, as indicated. **(I-K)** Non-autonomous effects of *dia-i*-induced depletion of source cytonemes on the number, length, and polarity of CD2:GFP-marked ASP cytonemes; K, Graph comparing ASP cytoneme numbers; dashed arrow, ASP tip cytonemes. **(L-N')** Non-autonomous effects of *dia-i*-induced depletion of ASP cytonemes (arrows) on source cytonemes; L,L',N,N', R-plots showing the correlation of ASP and source cytoneme number, length and orientation in control (L,L'; *w-) and btl>dia-i* condition (N,N'). **(O,P)** Non-autonomous effects of *Btl:DN*-induced depletion of ASP cytonemes (arrows) on source cytonemes: control, *btl-Gal4,UAS*-CD8GFP; *bnl-LexA,LexO*-mCherryCAAX x w^{-} (O); *btl-Gal4,UAS*-CD8GFP; *bnl-LexA,LexO*-mCherryCAAX x *UAS-Btl:DN* (P). **(F-P)** dashed arrow and arrow, non-autonomous and autonomous effects, respectively. All panels except F,G, live imaging. Scale bars, 20 µm.

Fig. 3. CAM-like Btl-Bnl binding leading to selective cell-cell adhesions. (A-C) Btl:DN-expressing ASP cytoneme numbers (arrow) highly correlated with the polarized *bnl*-source cytoneme numebrs (dashed arrow): Variable numbers of ASP cytonemes were produced by differential dominant-negative effects of Btl:DN (*btl-Gal4,UAS*-CD8GFP/+; *bnl-LexA,LexO*-mCherryCAAX/*UAS-Btl:DN*; see Methods); C, Graph showing the correlation between source and ASP cytonemes numbers in each disc (n=19). **(D,D')** Bnl^{ex} (blue, αBnl^{ex}) is asymmetrically enriched at the contact sites (arrowheads) between the source and Btl:DN-expressing ASP cytonemes; D', split αBnl^{ex} channel. (**E,E')** Btl-DN:Cherry puncta colocalized with Bnl^{ex} (green) on tracheal cytonemes. **(F)** Drawing depicting CAM assay using S2 cells. **(G-N)** Trans-pairing of S2-Bnl:GFP with either S2-Btl:Cherry (G-G",K,K') or S2-Btl:DN:Cherry (L-M') but not with S2-sBtl:Cherry control (N); dashed cell outline, trans-paired cells; arrow, trans-synaptic receptor-ligand co-clusters; dashed arrow, nucleus; dpERK (blue, αdpERK). **(H)** Graphs comparing the frequency of receptor-ligand trans-pairing (see Methods). **(I)** Graphs

comparing % of dpERK-positive Btl-expressing cells that are either trans-paired (for Btl:Cherry & Btl-DN:Cherry) or nearby (for sBtl:Cherry & Unpaired Btl:Cherry) to S2-Bnl:GFP; All panels except A,B: fixed cells/tissues. Scale bars, 20 μm; 10 μm (G-N).

Fig. 4. Post-translational Bnl cleavage and lipidation. (A,A') Schematic map of the Bnl protein (A) and hydrophobicity plot (A'): showing - signal peptide (SP), conserved FGF-domain (HSPG+FGFR binding), furin cleavage site (arrow), HA- (site #1), GFP- (site # 3), mCherry-tags, and putative SS (hydrophilic spacer - blue shade; hydrophobic tail - yellow shade). **(B-B''')** S2 cells expressing Bnl:GFP$_3$Cherry$_c$ (arrowheads); arrow, cleaved externalized Bnl:GFP$_3^{ex}$ portion probed with αGFP^{ex} (blue); dashed line, cell outline; split channels, indicated. **(C)** Wing disc expressing Bnl:GFP$_3$Cherry$_c$ under *bnl-Gal4*; arrow, intact protein (GFP+mCherry); short dashed lined area, *bnl*-source; open arrow, cleaved Bnl:GFP$_3$; ASP, long dashed line; blue, αDlg. **(D-G)** PIPLC shedding assay on S2 cells expressing various constructs: (D) Schematic depicting a GPI-AP and PIPLC cleavage site. (D') Surface-localized fractions of various proteins (GFP - total expression; red - surface fraction probed with αGFP^{ex} for GFP-tag; αBnl^{ex} for Bnl) with and without PIPLC; (E) Schematic maps of Bnl:GFP constructs used; (F,G) Graphs comparing the ratio of cell surface (red, αGFP^{ex} or αBnl^{ex} immuno-fluorescence) to total proteins (GFP fluorescence) (also see Fig. S3; S4A-G); surface expression of untagged Bnl was normalized with co-expressed CD8:GFP; ***, $p<0.001$. S2 cells co-transfected with *actin-Gal4* and *UAS-"X"*. Scale bars: 10 μm.

Fig. 5. Bnl is GPI-anchored to the wing disc source cell surface. (A-C) Wing discs (*w*$^-$) showing surface-localized native Bnl^{ex} (red, αBnl^{ex}) levels on the *bnl*-source area (arrows) before (A) and after (B) PIPLC treatment; C, graph showing significant shedding of Bnl^{ex} by PIPLC treatment. **(D-F)** Wing discs overexpressing Bnl under *bnl-Gal4* showing surface Bnl^{ex} (red, αBnl^{ex}) levels on the *bnl*-source (arrows) before (D) and after (E) PIPLC treatment; F, graphs showing shedding of Bnl^{ex} by PIPLC treatment. **(G-M)** Source surface levels (red, αGFP^{ex}) of Bnl:GFP, Bnl:GFPΔC and Bnl:GFPΔC-TM on wing discs when expressed under *bnl-Gal4* before and after PIPLC;

M, graph comparing the fraction of total protein (probed by GFP) localized on the source surface (red, αGFP^{ex}) before and after PIPLC treatment; n=5 for each; *, non-expressing source-surrounding disc area; dashed line, ASP or *bnl*-source; Scale bars, 30 μm.

Fig. 6. GPI-anchored Bnl drives CAM-like bidirectional contact matchmaking. (A-C) CAM-like trans-pairing of S2-Btl:Cherry with S2-Bnl:GFPΔC-TM (B,C) and S2-Bnl:GFP (C; Fig.3G,K) but not with S2-Bnl:GFPΔC (A,C); arrow, receptor-ligand co-clusters; open arrow, nucleus in trans-paired or proximal S2-Btl:Cherry; arrowhead, Bnl:GFP signal uptake into the juxtaposed or trans-paired S2-Btl:Cherry cell; blue, nuclear dpERK (αdpERK); C, graphs showing % of trans-paired cells. **(D-L)** Comparison of Bnl:GFP (control), Bnl:GFPΔC, or Bnl:GFPΔC-TM signals for induction of reciprocal polarity of ASP and source cytonemes (arrows), when expressed from the disc source (also see Fig.S6A-F); Genotypes, as indicated; D, inset, ROI (box) in green and blue channels; D,G,J, extended Z projection; E,E',H,K, 3D-rendered views; dashed lines, ASP; G,H, dashed arrows, randomly oriented short cytonemes; F,I,L, R-plots comparing numbers, length, and directionality of ASP and source cytonemes as indicated (see Fig. S6G). All panels except A,B, live imaging. Scale bars, 10μm (A,B), 20μm (D-K).

Fig. 7. CAM-like Btl-Bnl-interactions organize cytonemes and cytoneme contacts. (A-A") 3D projection (A,A'') and orthogonal view (A') of wing discs showing cytoneme-mediated adhesion between the ASP (*btl>CherryCAAX*) and the Bnl:GFPΔC-TM-expressing disc *bnl*-source (blue, *bnl>CD4:IFP2,*Bnl:GFPΔC-TM); arrows, Bnl:GFPΔC-TM-localized contact sites. **(B-C)** 3D-projected images of Bnl:GFPΔC-TM-expressing wing disc *bnl*-source (blue, *bnl>CD4:IFP2*) in *btl:cherry*^{endo} knock-in background (ASP expressed endogenous Btl:Cherry [9]), showing trans-synaptic co-clustering of Btl:Cherry^{endo} and Bnl:GFPΔC-TM puncta (arrows) at the inter-cytoneme contact sites. **(D,E)** Graphs showing dynamics of Bnl:GFPΔC-TM-exchanging ASP and source cytonemes (compare to control in Fig.1L-N and Table S1). **(F-J)** Randomly-localized wing disc clones (mCherryCAAX-marked) expressing Bnl:GFPΔC-TM, and their

cytoneme-dependent interactions (arrow) with the ASP (dashed line); F, an approximate map of clones in G-J; Open arrows, randomly oriented cytonemes. **(K-M')** Randomly-localized wing disc clones expressing Btl:GFP (*), and their cytoneme-dependent polarized interactions (arrow) with mCherryCAAX-marked *bnl*-source (genotypes: see Method; only the basal-most section of disc columnar cells shown); M', zoomed in ROI in M. All panels, live imaging. Scale bars, 20 μm.

Fig. 8. GPI anchor ensures Bnl release at the cytoneme contact sites. (A-E) Dispersion patterns of Bnl:GFP variants expressed under *bnl-Gal4* (*UAS-mCherryCAAX;bnl-Gal4* x *UAS-"X"*); D, Inset, split-colors of ROI (box); arrowhead, source cell membrane containing Bnl:GFPΔC-TM puncta in the ASP. (**F)** Schematic map of a Furin-sensor HA_1Bnl:GFP_3; red arrow, Furin cleavage site; black arrow, ΔC or TM modification sites; double-sided arrows, uncleaved HA_1Bnl:GFP_3 and cleaved Bnl:GFP_3 that were transferred to the ASP in the presence and absence of Fur inhibition, respectively. **(F')** Illustration depicting experimental strategy to detect ASP-specific dispersal rate of uncleaved signals in Furin-inhibited media. **(G-P)** Comparison of the ASP-specific uptake of HA_1Bnl:GFP_3, HA_1Bnl:GFP_3ΔC-TM, and HA_1Bnl:GFP_3ΔC (yellow puncta: red-αHA+green-GFP) from the disc source; P, Graphs, comparing the levels of uptake; each time point, an average of multiple samples (see Methods). **(Q-S)** Comparison of non-specific dispersion between HA_1Bnl:GFP_3 (Q) and HA_1Bnl:GFP_3ΔC (R,S) in ex vivo wing disc; All panels: dashed outline, ASP; arrow, cleaved Bnl:GFP_3; arrowhead, uncleaved signal; dashed arrow, source cells; αDlg, cell outlines; *, non-specific disc areas; G-S, only merged and corresponding red channels were shown. Scale bars, 20 μm.

Fig. 9. GPI-anchoring is required for long-range tissue-specific Bnl signaling patterns. (A-C) Comparison of the dispersion and signaling (dpERK, red; arrows) patterns of Bnl:GFP (control), Bnl:GFPΔC, and Bnl:GFPΔC-TM expressed from ectopic GOF clones within the ASP stalk and TC (approx. clone locations and dpERK patterns indicated in inset); genotype: *hsFlp*; *btlenh>y+>Gal4,btlenh-mRFPmoe* x *UAS-"X"*"); (also see Fig. S7E-G); arrow and arrowhead (B,B'), signal-recipient cells with and

without nuclear dpERK, respectively; D, Graphs comparing the percentage of signal-receiving ASP cells with nuclear dpERK (see Fig. S7G); OE, expression of Bnl:GFP variants in the *bnl* source (*bnlGa4 x UAS-X*; $p < 0.01$: ΔC (n = 16) vs either Bnl:GFP (n = 17) or TM (n = 13); see Fig. S7H-K). **(E-H)** Levels of tracheal branch invasion (arrows) into larval salivary glands ectopically expressing either Bnl:GFP (control), TM, or ΔC (*bnl-Gal4* X *UAS-X*); E-G, brightfield, 10X magnification; H, Graphs comparing frequency of terminal branching (see Methods). **(I-L)** Levels of ectopically expressed Bnl:GFP, TM, and ΔC displayed on the basal surface of the expressing salivary glands; L, graph comparing the fraction of surface-displayed signals (red/arrowhead, αGFP^{ex}) relative to the total protein (GFP level); arrow, cell junctions; $p < 0.05$: Bnl:GFP vs TM, $p < 0.01$: ΔC vs either Bnl:GFP or TM. Scale bars, 30 μm; 100 μm (E-G); 20 μm (I-K).

Fig.10. Bnl's GPI anchoring and its cytoneme-mediated bidirectional signaling. (A) Model illustrating the mechanisms of GPI anchoring and tissue-specific cytoneme contact assembly by the CAM-like bidirectional Btl-Bnl signaling, followed by the contact-dependent signal release for the MAPK signaling feedbacks; dashed arrow, putative CAM-like signaling feedbacks at the cell membrane. **(B-C)** Models illustrating the loss of polarized bidirectional signaling with BnlΔC (B) and the rescue of the contact-dependent bidirectional signaling responses by adding a TM-tether to BnlΔC (C).

References

1. Shilo, B.-Z. New Twists in Drosophila Cell Signaling*. *J Biol Chem* 291, 7805–7808 (2016).

2. Perrimon, N., Pitsouli, C. & Shilo, B.-Z. Signaling mechanisms controlling cell fate and embryonic patterning. *Cold Spring Harbor Perspectives in Biology* 4, a005975–a005975 (2012).

3. Housden, B. E. & Perrimon, N. Spatial and temporal organization of signaling pathways. *Trends Biochem Sci* 39, 457–464 (2014).

4. Zhang, C. & Scholpp, S. Cytonemes in development. *Curr Opin Genet Dev* 57, 25–30 (2019).

5. Roy, S., Huang, H., Liu, S. & Kornberg, T. B. Cytoneme-mediated contact-dependent transport of the Drosophila decapentaplegic signaling protein. *Science (New York, N.Y.)* 343, 1244624 (2014).

6. Bischoff, M. *et al.* Cytonemes are required for the establishment of a normal Hedgehog morphogen gradient in Drosophila epithelia. *Nat Cell Biol* 15, 10.1038/ncb2856 (2013).

7. González-Méndez, L., Gradilla, A.-C. & Guerrero, I. The cytoneme connection: direct long-distance signal transfer during development. *Development* 146, dev174607 (2019).

8. Kornberg, T. B. & Roy, S. Communicating by touch--neurons are not alone. *Trends in cell biology* 24, 370–376 (2014).

9. Du, L., Sohr, A., Yan, G. & Roy, S. Feedback regulation of cytoneme-mediated transport shapes a tissue-specific FGF morphogen gradient. (2018).

10. Chen, W., Huang, H., Hatori, R. & Kornberg, T. B. Essential basal cytonemes take up Hedgehog in the Drosophila wing imaginal disc. *Development (Cambridge, England)* 144, 3134–3144 (2017).

11. Hall, E. T. *et al.* Cytoneme delivery of Sonic Hedgehog from ligand-producing cells requires Myosin 10 and a Dispatched-BOC/CDON co-receptor complex. *eLife* 10, (2021).

12. Huang, H. & Kornberg, T. B. Myoblast cytonemes mediate Wg signaling from the wing imaginal disc and Delta-Notch signaling to the air sac primordium. *Elife* 4, e06114 (2015).

13. Roy, S., Hsiung, F. & Kornberg, T. B. Specificity of Drosophila Cytonemes for Distinct Signaling Pathways. *Science (New York, N.Y.)* 332, 354–358 (2011).

14. Stanganello, E. *et al.* Filopodia-based Wnt transport during vertebrate tissue patterning. *Nat Commun* 6, 5846 (2015).

15. Sanders, T. A., Llagostera, E. & Barna, M. Specialized filopodia direct long-range transport of SHH during vertebrate tissue patterning. *Nature* 497, 628–632 (2013).

16. Eom, D. S. & Parichy, D. M. A macrophage relay for long-distance signaling during postembryonic tissue remodeling. *Science (New York, N.Y.)* 355, 1317–1320 (2017).

17. Inaba, M., Buszczak, M. & Yamashita, Y. M. Nanotubes mediate niche-stem cell signaling in the Drosophila testis. *Nature* 523, 329–332 (2015).

18. Fereres, S., Hatori, R., Hatori, M. & Kornberg, T. B. Cytoneme-mediated signaling essential for tumorigenesis. *Plos Genet* 15, e1008415 (2019).

19. Krupke, O. A., Zysk, I., Mellott, D. O. & Burke, R. D. Eph and Ephrin function in dispersal and epithelial insertion of pigmented immunocytes in sea urchin embryos. *Elife* 5, e16000 (2016).

20. Sato, M. & Kornberg, T. B. FGF Is an Essential Mitogen and Chemoattractant for the Air Sacs of the Drosophila Tracheal System. *Dev Cell* 3, 195–207 (2002).

21. Sutherland, D., Samakovlis, C. & Krasnow, M. A. branchless encodes a Drosophila FGF homolog that controls tracheal cell migration and the pattern of branching. *Cell* 87, 1091–1101 (1996).

22. Klämbt, C., Glazer, L. & Shilo, B. Z. breathless, a Drosophila FGF receptor homolog, is essential for migration of tracheal and specific midline glial cells. *Gene Dev* 6, 1668–1678 (1992).

23. Egea, J. & Klein, R. Bidirectional Eph–ephrin signaling during axon guidance. *Trends in cell biology* 17, 230–238 (2007).

24. Hynes, R. O. Integrins: bidirectional, allosteric signaling machines. *Cell* 110, 673–687 (2002).

25. Kalappurakkal, J. M. *et al.* Integrin Mechano-chemical Signaling Generates Plasma Membrane Nanodomains that Promote Cell Spreading. *Cell* 177, 1738-1756.e23 (2019).

26. Saha, S., Anilkumar, A. A. & Mayor, S. GPI-anchored protein organization and dynamics at the cell surface. *J Lipid Res* 57, 159–175 (2016).

27. Gowrishankar, K. *et al.* Active Remodeling of Cortical Actin Regulates Spatiotemporal Organization of Cell Surface Molecules. *Cell* 149, 1353–1367 (2012).

28. Raghupathy, R. *et al.* Transbilayer Lipid Interactions Mediate Nanoclustering of Lipid-Anchored Proteins. *Cell* 161, 581–594 (2015).

29. Um, J. W. & Ko, J. Neural Glycosylphosphatidylinositol-Anchored Proteins in Synaptic Specification. *Trends in cell biology* 27, 931–945 (2017).

30. Schwank, G. *et al.* Formation of the long range Dpp morphogen gradient. *PLoS Biology* 9, e1001111 (2011).

31. González-Méndez, L., Seijo-Barandiarán, I. & Guerrero, I. Cytoneme-mediated cell-cell contacts for Hedgehog reception. *Elife* 6, e24045 (2017).

32. Mattes, B. & Scholpp, S. Emerging role of contact-mediated cell communication in tissue development and diseases. *Histochemistry and cell biology* 150, 431–442 (2018).

33. Kohsaka, H. & Nose, A. Target recognition at the tips of postsynaptic filopodia: accumulation and function of Capricious. *Development (Cambridge, England)* 136, 1127–1135 (2009).

34. Sanes, J. R. & Zipursky, S. L. Synaptic Specificity, Recognition Molecules, and Assembly of Neural Circuits. *Cell* 181, 1434–1435 (2020).

35. Gilmour, D., Rembold, M. & Leptin, M. From morphogen to morphogenesis and back. *Nature* 541, 311–320 (2017).

36. Dustin, M. L. The Immunological Synapse. *Cancer Immunol Res* 2, 1023–1033 (2014).

37. Sohr, A., Du, L., Wang, R., Lin, L. & Roy, S. Drosophila FGF cleavage is required for efficient intracellular sorting and intercellular dispersal. *J Cell Biol* 218, 1653–1669 (2019).

38. Kinoshita, T. & Fujita, M. Biosynthesis of GPI-anchored proteins: special emphasis on GPI lipid remodeling. *Journal of Lipid Research* 57, 6–24 (2016).

39. Zurzolo, C. & Simons, K. Glycosylphosphatidylinositol-anchored proteins: Membrane organization and transport. *Biochimica Et Biophysica Acta Bba - Biomembr* 1858, 632–639 (2016).

40. Caras, I. W. An internally positioned signal can direct attachment of a glycophospholipid membrane anchor. *J Cell Biology* 113, 77–85 (1991).

41. Ferguson, M. A., Kinoshita, T. & Hart, G. W. *Glycosylphosphatidylinositol Anchors*. (Cold Spring Harbor (NY): Cold Spring Harbor Laboratory Press, 2015). doi:doi: 10.1101/glycobiology.3e.012.

42. Greco, V., Hannus, M. & Eaton, S. Argosomes: a potential vehicle for the spread of morphogens through epithelia. *Cell* 106, 633–645 (2001).

43. Miura, G. I. *et al.* Palmitoylation of the EGFR ligand Spitz by Rasp increases Spitz activity by restricting its diffusion. *Developmental Cell* 10, 167–176 (2006).

44. Yan, D. & Lin, X. Drosophila glypican Dally-like acts in FGF-receiving cells to modulate FGF signaling during tracheal morphogenesis. *Dev Biol* 312, 203–216 (2007).

45. Böhme, U. & Cross, G. A. M. Mutational analysis of the variant surface glycoprotein GPI-anchor signal sequence in Trypanosoma brucei. *J Cell Sci* 115, 805–16 (2002).

46. Delahunty, M. D., Stafford, F. J., Yuan, L. C., Shaz, D. & Bonifacino, J. S. Uncleaved signals for glycosylphosphatidylinositol anchoring cause retention of precursor proteins in the endoplasmic reticulum. *J Biol Chem* 268, 12017–12027 (1993).

47. Incardona, J. P. & Rosenberry, T. L. Replacement of the glycoinositol phospholipid anchor of Drosophila acetylcholinesterase with a transmembrane domain does not alter sorting in neurons and epithelia but results in behavioral defects. *Mol Biol Cell* 7, 613–630 (1996).

48. Ochoa-Espinosa, A. & Affolter, M. Branching Morphogenesis: From Cells to Organs and Back. *Csh Perspect Biol* 4, a008243 (2012).

49. Jarecki, J., Johnson, E. & Krasnow, M. A. Oxygen Regulation of Airway Branching in Drosophila Is Mediated by Branchless FGF. *Cell* 99, 211–220 (1999).

50. Du, L. *et al.* Unique patterns of organization and migration of FGF-expressing cells during Drosophila morphogenesis. *Dev Biol* 427, 35–48 (2017).

51. Lichtenthaler, S. F. Sheddase Gets Guidance. *Science (New York, N.Y.)* 335, 179–180 (2012).

52. Stepanik, V., Sun, J. & Stathopoulos, A. FGF Pyramus Has a Transmembrane Domain and Cell-Autonomous Function in Polarity. *Current biology : CB* (2020).

53. Lee, J. J. *et al.* Autoproteolysis in hedgehog Protein Biogenesis. *Science* 266, 1528–1537 (1994).

54. Willert, K. *et al.* Wnt proteins are lipid-modified and can act as stem cell growth factors. *Nature* 423, 448–452 (2003).

55. Taylor, F. R. *et al.* Enhanced potency of human Sonic hedgehog by hydrophobic modification. *Biochemistry* 40, 4359–4371 (2001).

56. Gallet, A., Ruel, L., Staccini-Lavenant, L. & Thérond, P. P. Cholesterol modification is necessary for controlled planar long-range activity of Hedgehog in Drosophila epithelia. *Development* 133, 407–418 (2006).

57. Callejo, A., Torroja, C., Quijada, L. & Guerrero, I. Hedgehog lipid modifications are required for Hedgehog stabilization in the extracellular matrix. *Development* 133, 471–483 (2006).

58. Speer, K. F. *et al.* Non-acylated Wnts Can Promote Signaling. *CellReports* 26, 875-883.e5 (2019).

59. Alexandre, C., Baena-Lopez, A. & Vincent, J.-P. Patterning and growth control by membrane-tethered Wingless. *Nature* 505, 180–185 (2014).

60. Yan, D. & Lin, X. Shaping morphogen gradients by proteoglycans. *Cold Spring Harbor Perspectives in Biology* 1, a002493–a002493 (2009).

61. Dejima, K., Kanai, M. I., Akiyama, T., Levings, D. C. & Nakato, H. Novel contact-dependent bone morphogenetic protein (BMP) signaling mediated by heparan sulfate proteoglycans. *The Journal of biological chemistry* 286, 17103–17111 (2011).

62. Balasubramanian, R. & Zhang, X. Mechanisms of FGF gradient formation during embryogenesis. *Semin Cell Dev Biol* 53, 94–100 (2016).

63. Huang, H. & Kornberg, T. B. Cells must express components of the planar cell polarity system and extracellular matrix to support cytonemes. *Elife* 5, e18979 (2016).

64. González-Mendez, L., Seijo-Barandiaŕan, I. & Guerrero, I. Cytoneme-mediated cell-cell contacts for Hedgehog reception. *eLife* 6, 605 (2017).

65. Simon, E. *et al*. Glypicans define unique roles for the Hedgehog co-receptors boi and ihog in cytoneme-mediated gradient formation. *Elife* 10, e64581 (2021).

66. Sohr, A., Du, L. & Roy, S. Ex vivo Drosophila Wing Imaginal Disc Culture and Furin Inhibitor Assay. *Bio-protocol* 9, e3336 (2019).

67. Chen, W., Huang, H., Hatori, R. & Kornberg, T. B. Essential basal cytonemes take up Hedgehog in the Drosophila wing imaginal disc. *Development* 144, 3134–3144 (2017).

Figure 1

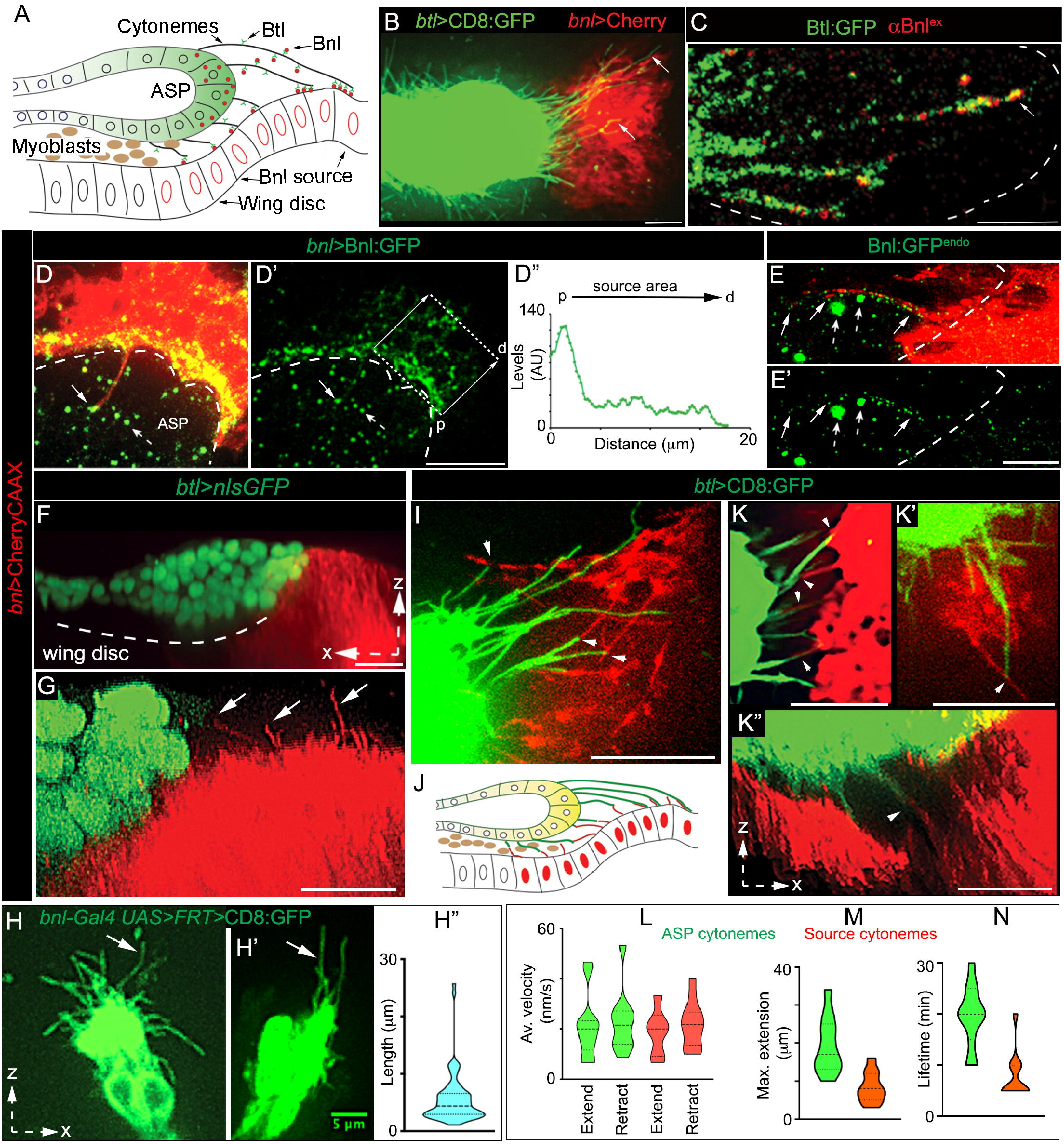
A
Cytonemes
Btl
Bnl
ASP
Myoblasts
Bnl source
Wing disc
B btl>CD8:GFP bnl>Cherry
C Btl:GFP αBnl^ex
bnl>Bnl:GFP
D
ASP
D'
d
p
D''
source area
p
d
140
Levels (AU)
0
0
Distance (μm)
20
Bnl:GFP^endo
E
E'
bnl>CherryCAAX
btl>nlsGFP
F
z
x
wing disc
G
btl>CD8:GFP
I
K
K'
K''
z
x
J
H bnl-Gal4 UAS>FRT>CD8:GFP
H'
z
x
5 μm
H''
30
Length (μm)
0
L
ASP cytonemes
M
Source cytonemes
N
60
Av. velocity (nm/s)
0
Extend
Retract
Extend
Retract
40
Max. extension (μm)
0
30
Lifetime (min)
0

Figure 2

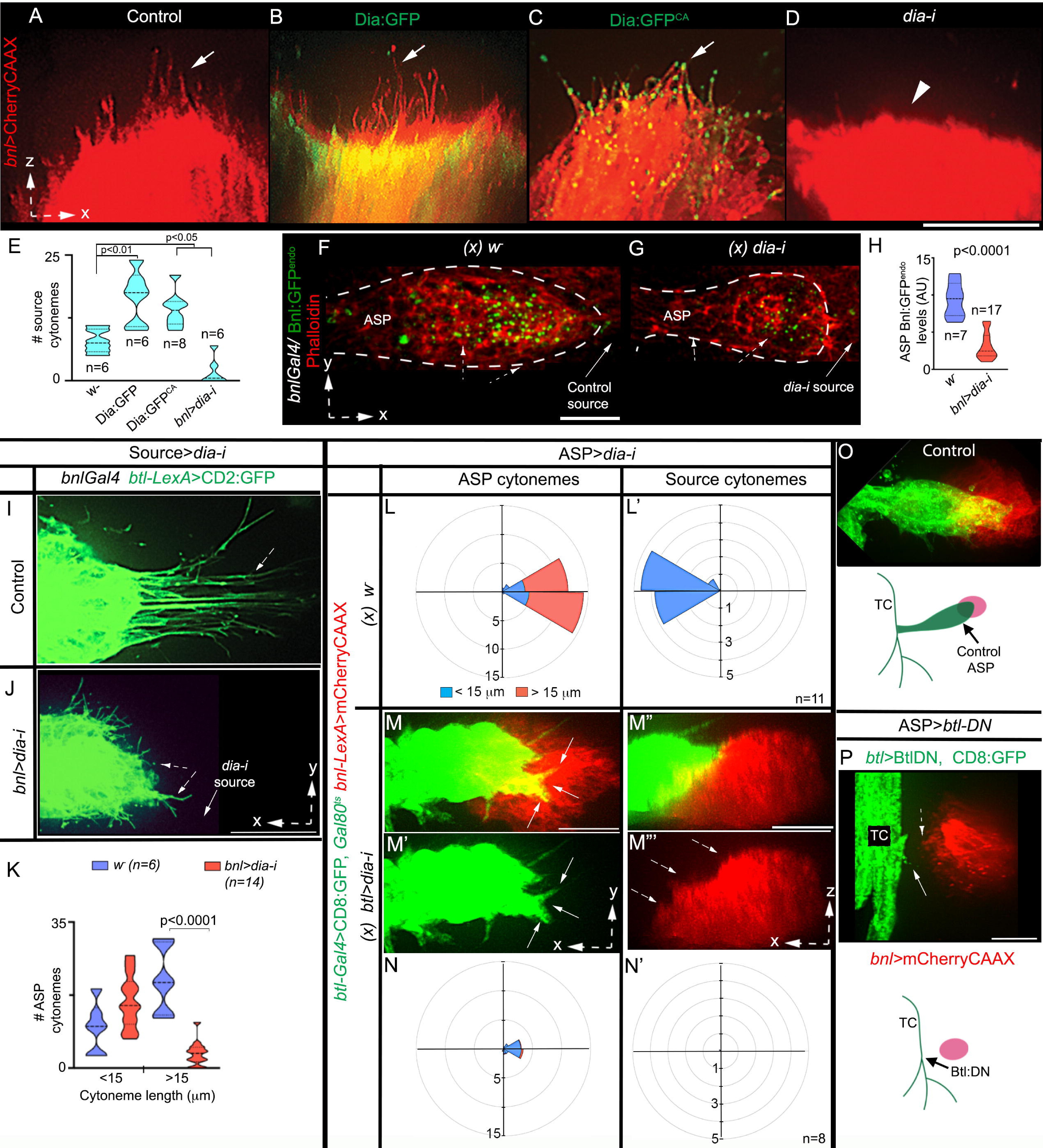
A Control
B Dia:GFP
C Dia:GFP^CA
D dia-i
bnl>CherryCAAX
z
x
E
# source cytonemes
25
0
p<0.01
p<0.05
n=6
n=6
n=8
n=6
w-
Dia:GFP
Dia:GFP^CA
bnl>dia-i
F (x) w-
G (x) dia-i
bnlGal4/ Bnl:GFP^endo Phalloidin
ASP
ASP
Control source
dia-i source
y
x
H
p<0.0001
ASP Bnl:GFP^endo levels (AU)
15
0
n=7
n=17
w-
bnl>dia-i
Source>dia-i
bnlGal4 btl-LexA>CD2:GFP
I Control
J bnl>dia-i
dia-i source
y
x
K
w- (n=6)
bnl>dia-i (n=14)
35
0
p<0.0001
# ASP cytonemes
<15
>15
Cytoneme length (μm)
ASP>dia-i
ASP cytonemes
Source cytonemes
btl-Gal4>CD8:GFP, Gal80^ts bnl-LexA>mCherryCAAX
(x) w-
(x) btl>dia-i
L
5
10
15
< 15 μm
> 15 μm
L'
1
3
5
n=11
M
M'
M''
M'''
y
x
z
x
N
5
15
N'
1
3
5
n=8
O Control
TC
Control ASP
ASP>btl-DN
P btl>BtlDN, CD8:GFP
TC
bnl>mCherryCAAX
TC
Btl:DN

Figure 3

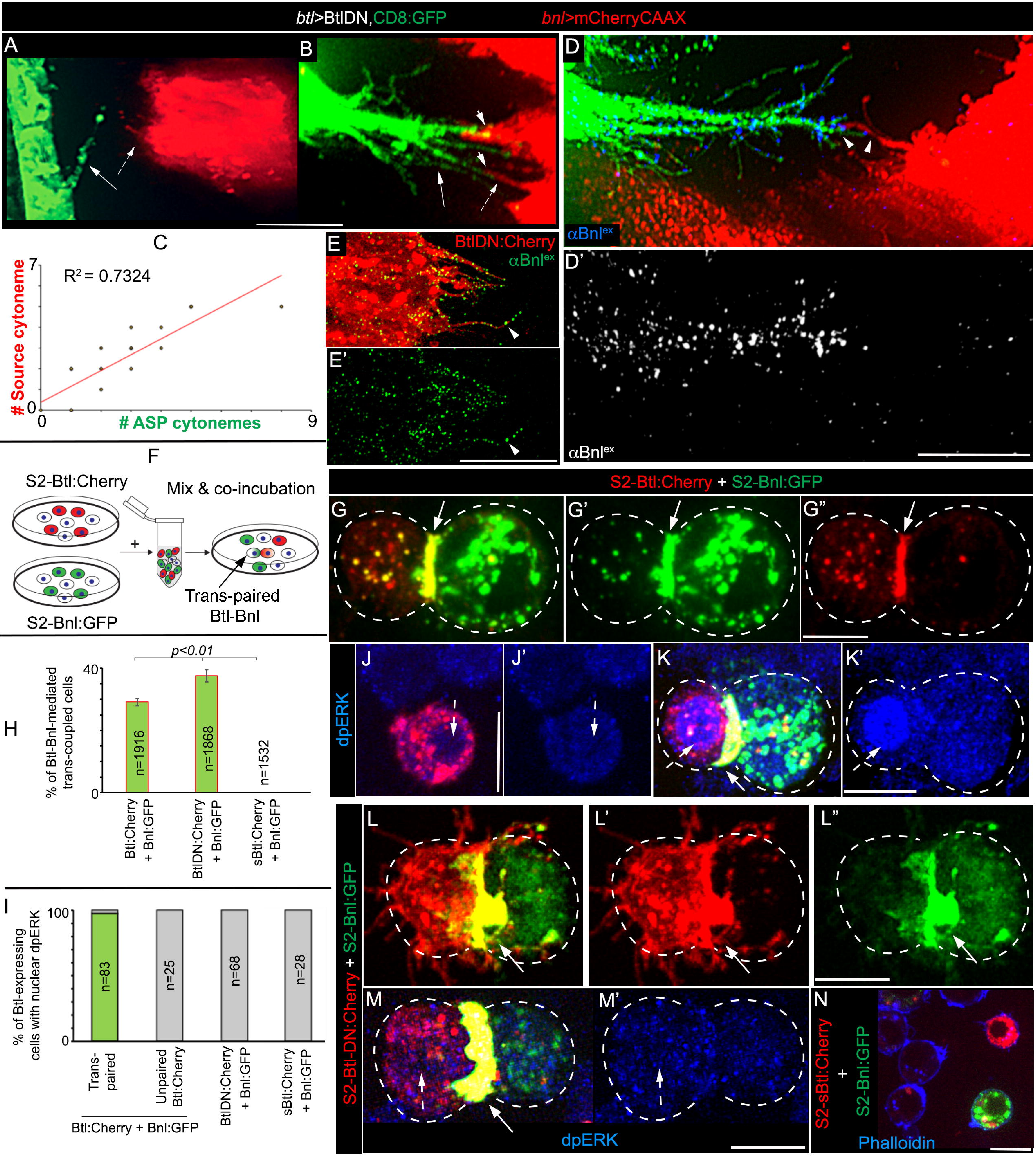
btl>BtlDN,CD8:GFP
bnl>mCherryCAAX
A
B
C
R² = 0.7324
# Source cytoneme
# ASP cytonemes
0
7
0
9
D
αBnl^ex
D'
αBnl^ex
E
BtlDN:Cherry
αBnl^ex
E'
F
S2-Btl:Cherry
Mix & co-incubation
+
Trans-paired Btl-Bnl
S2-Bnl:GFP
S2-Btl:Cherry + S2-Bnl:GFP
G
G'
G''
H
% of Btl-Bnl-mediated trans-coupled cells
p<0.01
40
0
n=1916
n=1868
n=1532
Btl:Cherry + Bnl:GFP
BtlDN:Cherry + Bnl:GFP
sBtl:Cherry + Bnl:GFP
dpERK
J
J'
K
K'
I
% of Btl-expressing cells with nuclear dpERK
100
0
n=83
n=25
n=68
n=28
Trans-paired
Unpaired Btl:Cherry
Btl:Cherry + Bnl:GFP
BtlDN:Cherry + Bnl:GFP
sBtl:Cherry + Bnl:GFP
S2-Btl-DN:Cherry + S2-Bnl:GFP
L
L'
L''
M
M'
dpERK
N
S2-sBtl:Cherry + S2-Bnl:GFP
Phalloidin

Figure 4

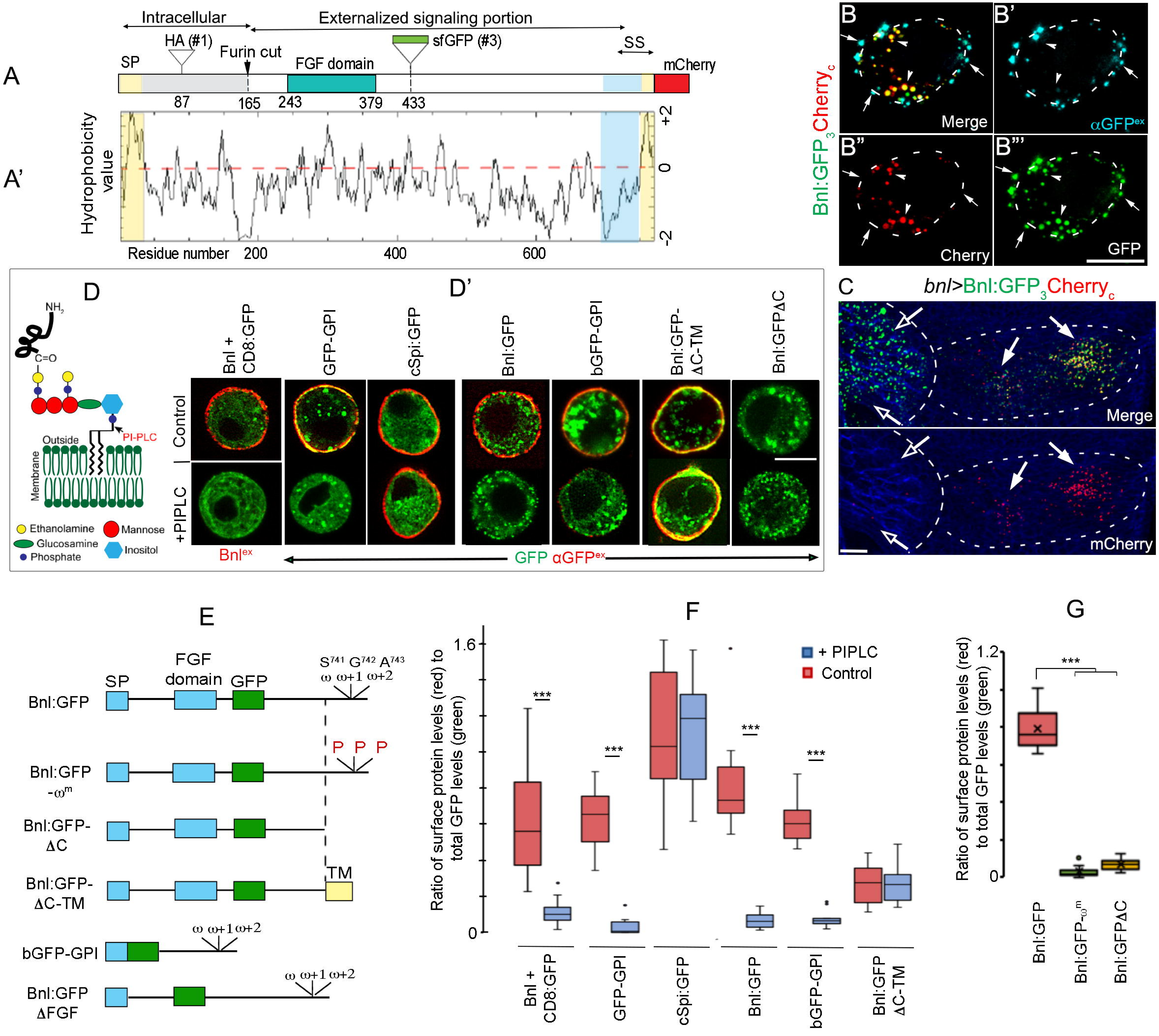
A
Intracellular
Externalized signaling portion
SP
HA (#1)
Furin cut
FGF domain
sfGFP (#3)
SS
mCherry
87
165
243
379
433
A'
Hydrophobicity value
Residue number
200
400
600
+2
0
-2
B
Merge
B'
αGFP^ex
B''
Cherry
B'''
GFP
Bnl:GFP3Cherryc
C
bnl>Bnl:GFP3Cherryc
Merge
mCherry
D
NH2
C=O
PI-PLC
Outside
Membrane
Ethanolamine
Mannose
Glucosamine
Phosphate
Inositol
D'
Bnl + CD8:GFP
GFP-GPI
cSpi:GFP
Bnl:GFP
bGFP-GPI
Bnl:GFP-ΔC-TM
Bnl:GFPΔC
Control
+PIPLC
Bnl^ex
GFP αGFP^ex
E
SP
FGF domain
GFP
S741 G742 A743
ω ω+1 ω+2
Bnl:GFP
P P P
Bnl:GFP-ω^m
Bnl:GFP-ΔC
TM
Bnl:GFP-ΔC-TM
bGFP-GPI
ω ω+1 ω+2
Bnl:GFP ΔFGF
ω ω+1 ω+2
F
Ratio of surface protein levels (red) to total GFP levels (green)
1.6
0
***
+ PIPLC
Control
Bnl + CD8:GFP
GFP-GPI
cSpi:GFP
Bnl:GFP
bGFP-GPI
Bnl:GFP ΔC-TM
G
Ratio of surface protein levels (red) to total GFP levels (green)
1.2
0
***
Bnl:GFP
Bnl:GFP-ω^m
Bnl:GFPΔC

Figure 5

w-
A
B
Control
+PIPLC
Bnl^ex
Phalloidin
C
p<0.01
35
0
Bnl^ex density on the source (AU)
n=6
n=7
Control
+ PIPLC
bnl-Gal4>Bnl
D
E
Control
+PIPLC
Bnl^ex
Phalloidin
F
p < 0.0001
140
0
Bnl^ex density on the source (AU)
n=13
n=9
Control
+ PIPLC
Bnl:GFP
Bnl:GFP^ex
Bnl:GFP-ΔC
Bnl:GFP-ΔC^ex
Bnl:GFPΔC-TM
Bnl:GFPΔC-TM^ex
Control
+PIPLC
G
H
I
J
K
L
Merge
split (red)
Merge
split (red)
Merge
split (red)
M
Fractions of surface (red) to total GFP levels on the source
1.2
0
p < 0.05
p < 0.01
Bnl:GFP
Bnl:GFP -ΔC
Bnl:GFΔC -TM
Control
+ PIPLC

Figure 6

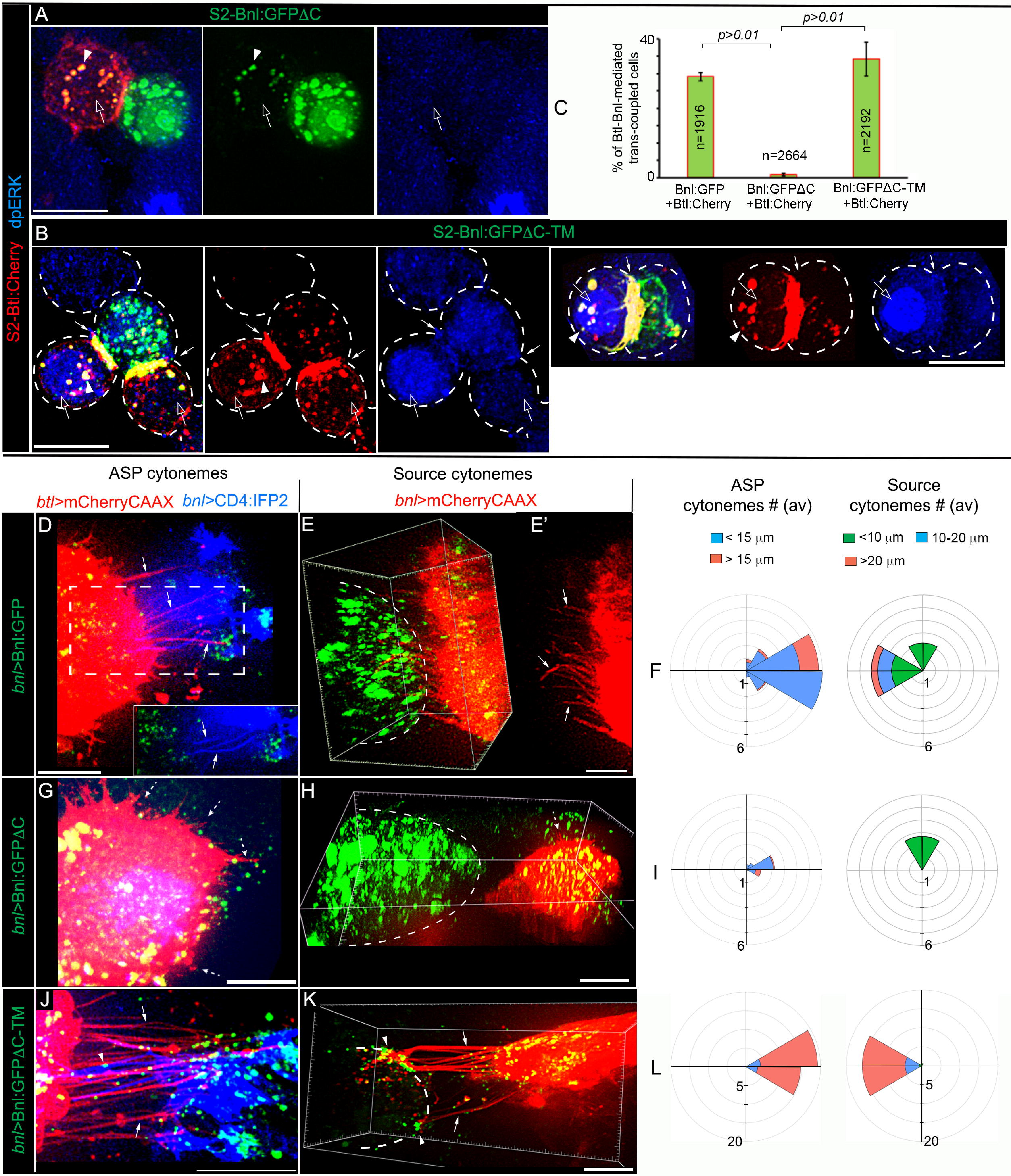
A
S2-Bnl:GFPΔC
S2-Btl:Cherry dpERK
C
p>0.01
p>0.01
40
0
% of Btl-Bnl-mediated trans-coupled cells
n=1916
n=2664
n=2192
Bnl:GFP +Btl:Cherry
Bnl:GFPΔC +Btl:Cherry
Bnl:GFPΔC-TM +Btl:Cherry
B
S2-Bnl:GFPΔC-TM
ASP cytonemes
btl>mCherryCAAX bnl>CD4:IFP2
Source cytonemes
bnl>mCherryCAAX
ASP cytonemes # (av)
< 15 µm
> 15 µm
Source cytonemes # (av)
<10 µm
10-20 µm
>20 µm
D
E
E'
F
1
6
1
6
bnl>Bnl:GFP
G
H
I
1
6
1
6
bnl>Bnl:GFPΔC
J
K
L
5
20
5
20
bnl>Bnl:GFPΔC-TM

Figure 7

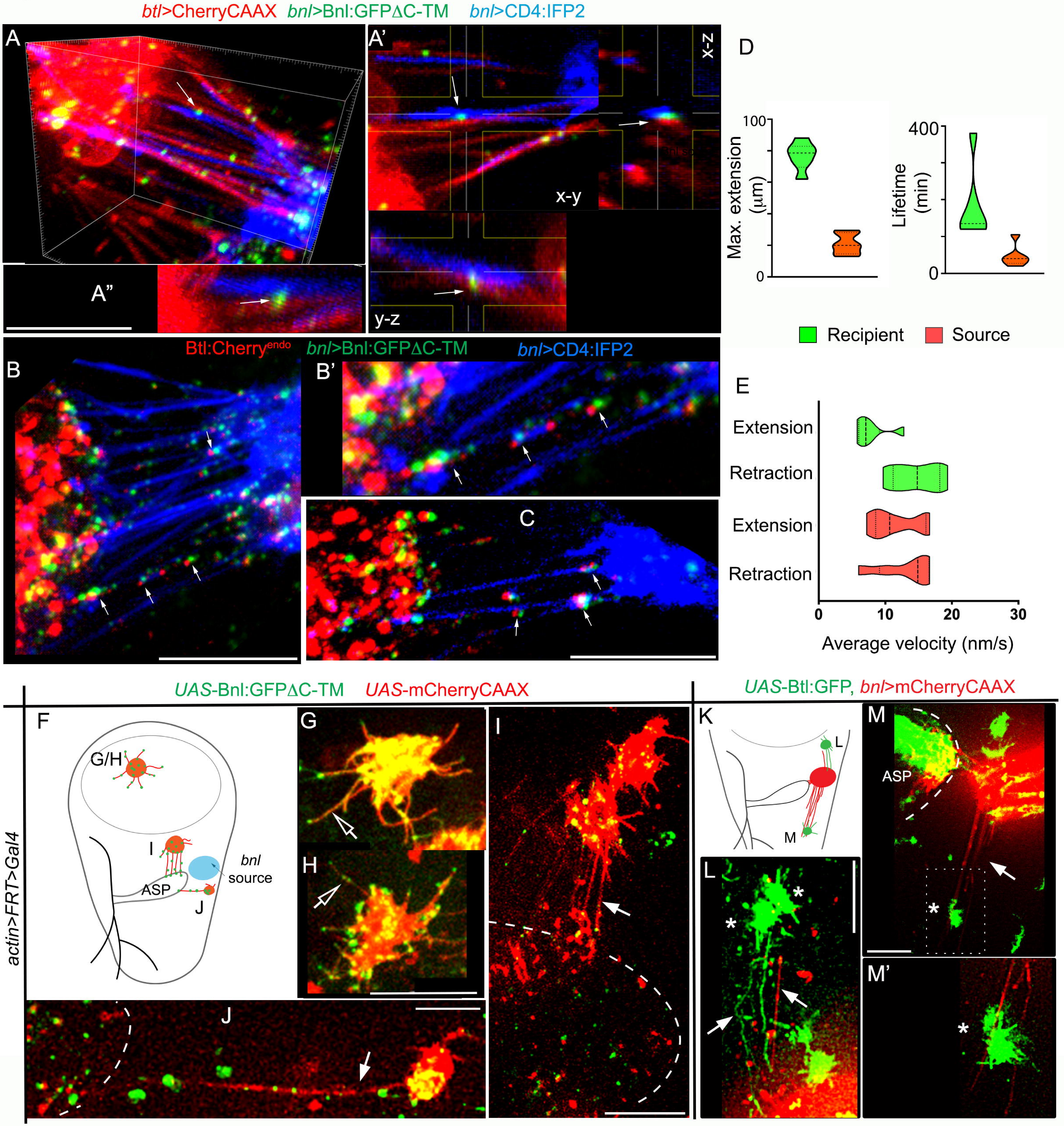
btl>CherryCAAX bnl>Bnl:GFPΔC-TM bnl>CD4:IFP2
A
A'
x-z
x-y
y-z
A"
D
100
0
Max. extension (µm)
400
0
Lifetime (min)
Recipient
Source
Btl:Cherry^endo bnl>Bnl:GFPΔC-TM bnl>CD4:IFP2
B
B'
C
E
Extension
Retraction
Extension
Retraction
0
10
20
30
Average velocity (nm/s)
UAS-Bnl:GFPΔC-TM UAS-mCherryCAAX
actin>FRT>Gal4
F
G/H
I
ASP
J
bnl source
G
H
I
J
UAS-Btl:GFP, bnl>mCherryCAAX
K
L
M
L
M
ASP
M'

Figure 8

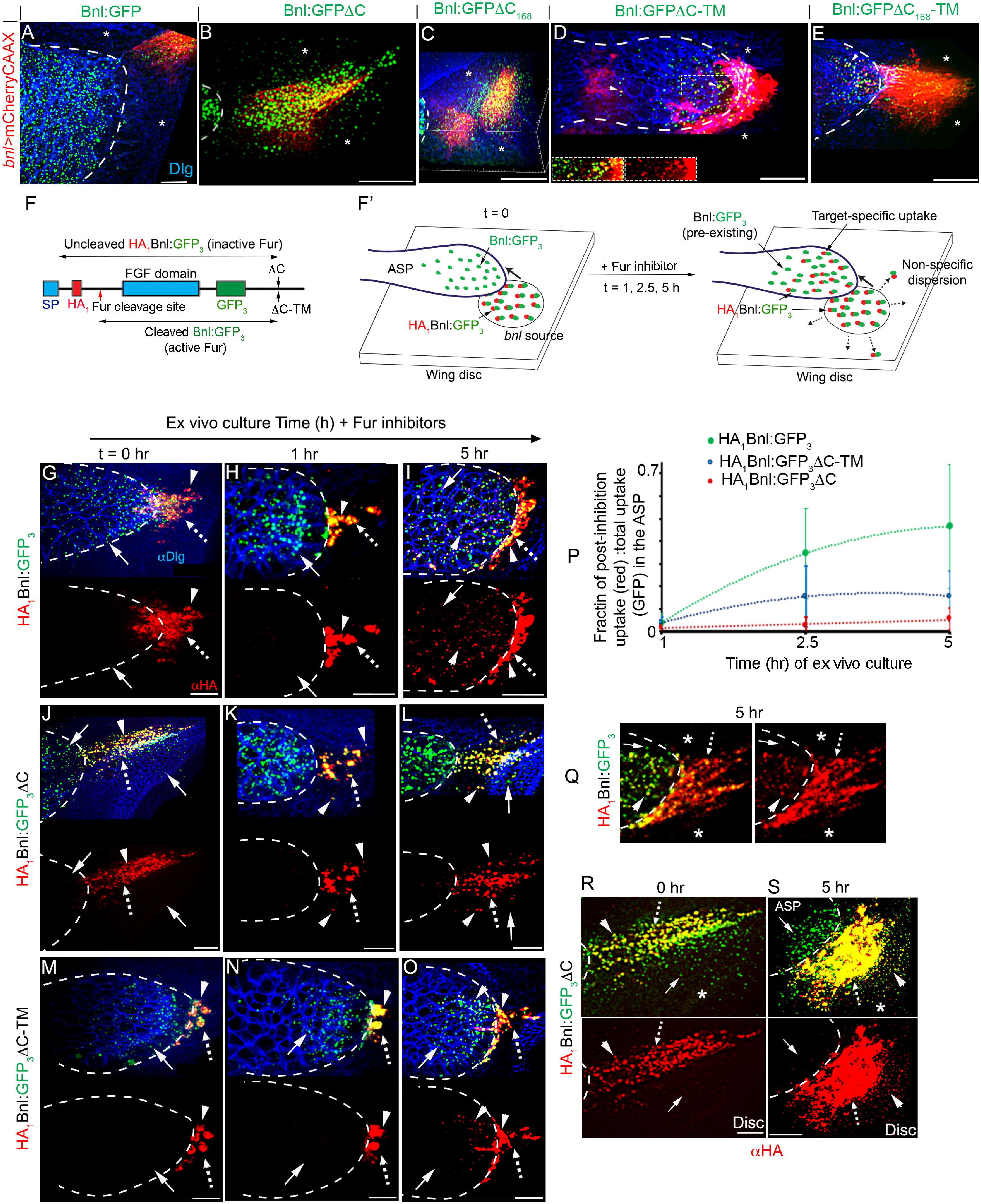
bnl>mCherryCAAX
Bnl:GFP
Bnl:GFPΔC
Bnl:GFPΔC168
Bnl:GFPΔC-TM
Bnl:GFPΔC168-TM
A
B
C
D
E
Dlg
F
Uncleaved HA1Bnl:GFP3 (inactive Fur)
FGF domain
ΔC
SP
HA1
Fur cleavage site
GFP3
ΔC-TM
Cleaved Bnl:GFP3
(active Fur)
F'
t = 0
Bnl:GFP3
ASP
HA1Bnl:GFP3
bnl source
Wing disc
+ Fur inhibitor
t = 1, 2.5, 5 h
Bnl:GFP3
(pre-existing)
Target-specific uptake
Non-specific dispersion
HA1Bnl:GFP3
Wing disc
Ex vivo culture Time (h) + Fur inhibitors
t = 0 hr
1 hr
5 hr
G
H
I
αDlg
αHA
HA1Bnl:GFP3
J
K
L
HA1Bnl:GFP3ΔC
M
N
O
HA1Bnl:GFP3ΔC-TM
HA1Bnl:GFP3
HA1Bnl:GFP3ΔC-TM
HA1Bnl:GFP3ΔC
P
Fractin of post-inhibition uptake (red) :total uptake (GFP) in the ASP
0.7
0
1
2.5
5
Time (hr) of ex vivo culture
5 hr
Q
HA1Bnl:GFP3
R
0 hr
S
5 hr
ASP
HA1Bnl:GFP3ΔC
Disc
Disc
αHA

Figure 9

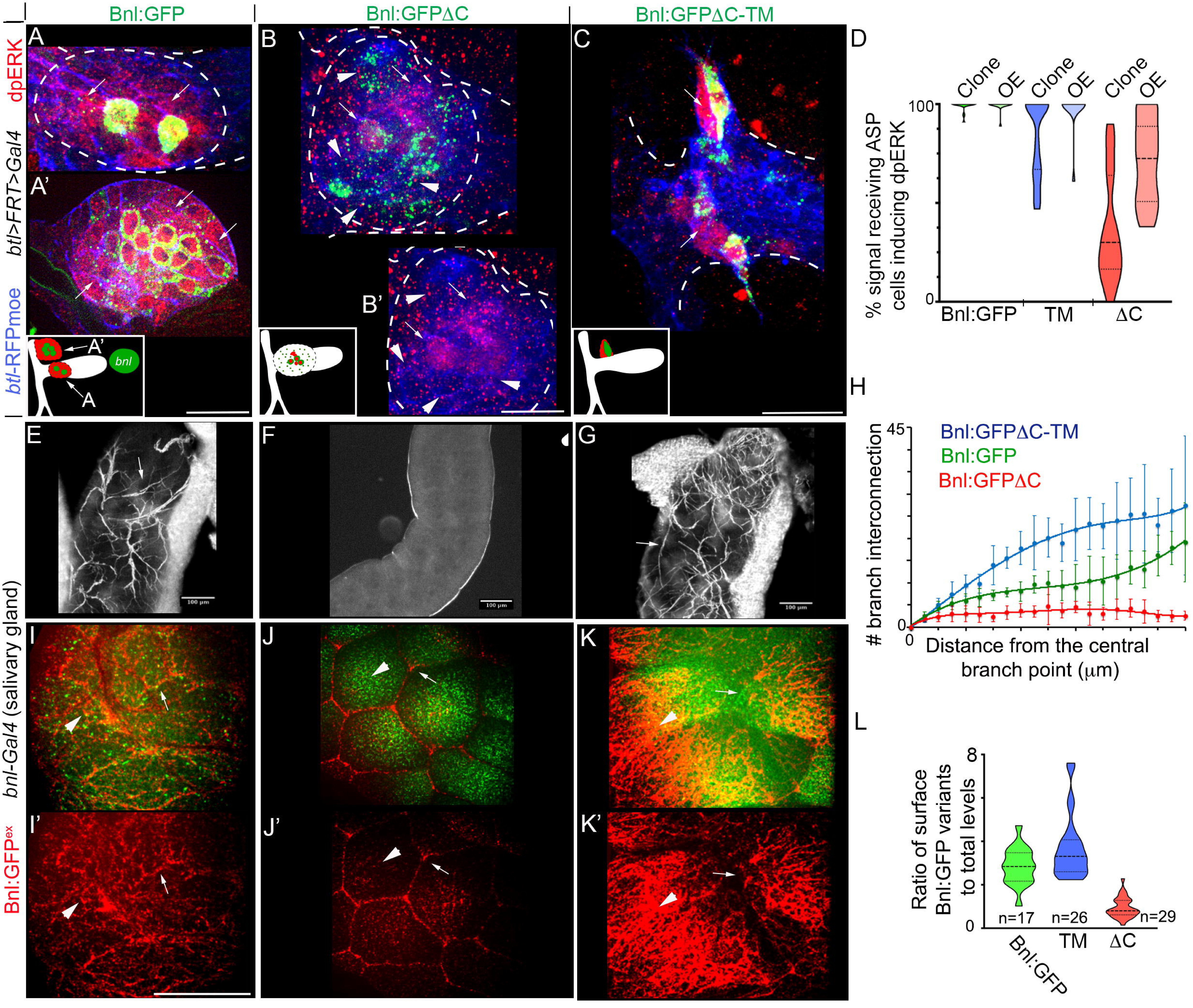
Bnl:GFP
Bnl:GFPΔC
Bnl:GFPΔC-TM
A
A'
B
B'
C
D
dpERK
btl>FRT>Gal4
btl-RFPmoe
bnl
Clone
OE
Clone
OE
Clone
OE
100
0
% signal receiving ASP cells inducing dpERK
Bnl:GFP
TM
ΔC
E
F
G
H
100 µm
100 µm
100 µm
Bnl:GFPΔC-TM
Bnl:GFP
Bnl:GFPΔC
45
0
0
# branch interconnection
Distance from the central branch point (µm)
bnl-Gal4 (salivary gland)
Bnl:GFPex
I
I'
J
J'
K
K'
L
Ratio of surface Bnl:GFP variants to total levels
8
0
n=17
n=26
n=29
Bnl:GFP
TM
ΔC

Figure 10

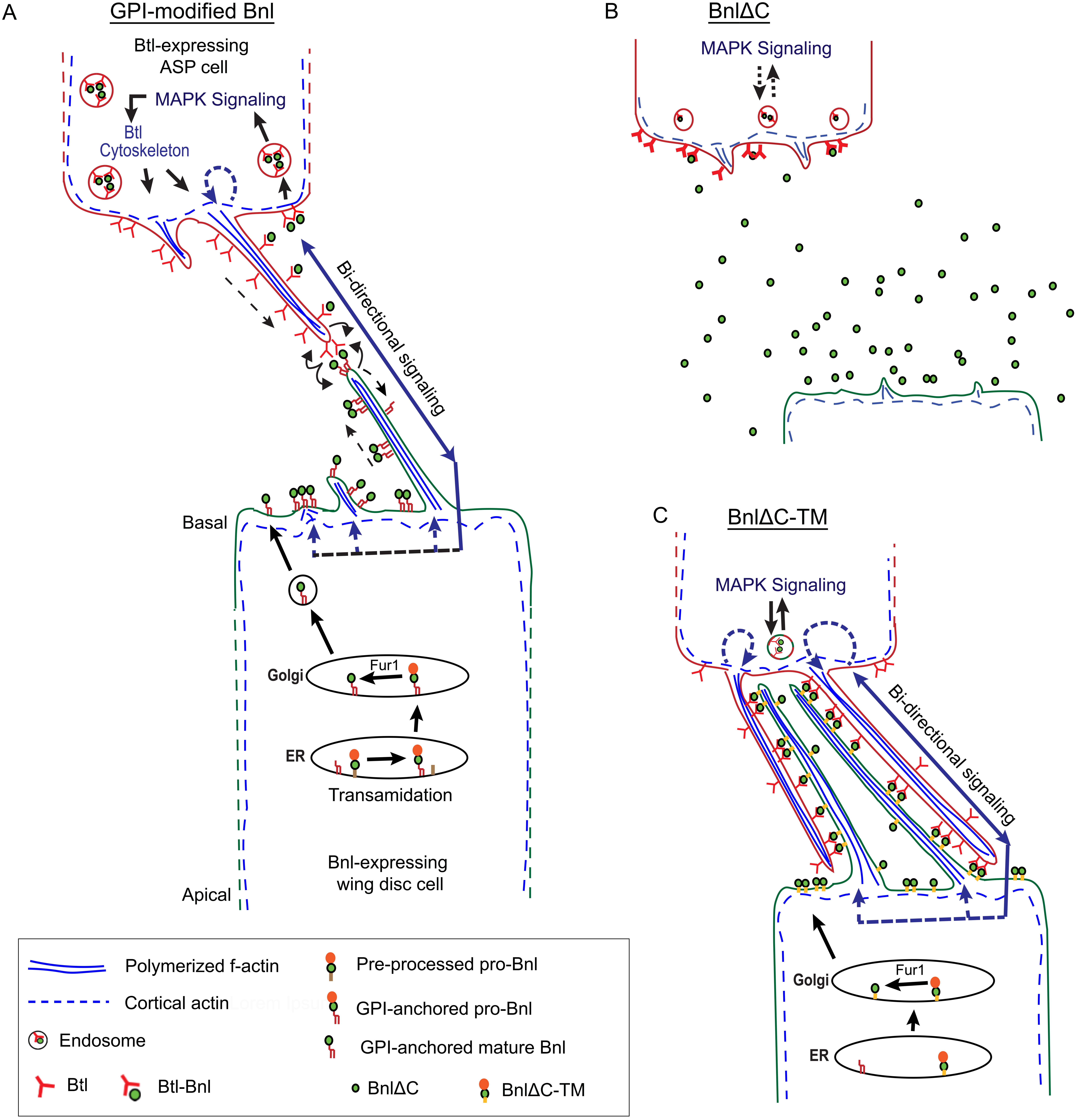
A
GPI-modified Bnl
Btl-expressing
ASP cell
MAPK Signaling
Btl
Cytoskeleton
Bi-directional signaling
Basal
Golgi
Fur1
ER
Transamidation
Bnl-expressing
wing disc cell
Apical
B
BnlΔC
MAPK Signaling
C
BnlΔC-TM
MAPK Signaling
Bi-directional signaling
Golgi
Fur1
ER
Polymerized f-actin
Cortical actin
Endosome
Btl
Btl-Bnl
Pre-processed pro-Bnl
GPI-anchored pro-Bnl
GPI-anchored mature Bnl
BnlΔC
BnlΔC-TM